ORIGINAL RESEARCH ARTICLE

The Relative Importance of Creep Hardening, Softening, and Damage in the Determination of Creep Failure Using a Monkman–Grant-Type Relation Derived Within the 4-θ Methodology

M. EVANS

An analysis of minimum creep rates *vs*. time to failure is a suggested approach to the evaluation of long-term creep rupture. But this requires constancy of this relation over all test conditions. This paper therefore used the 4-θ methodology to study in more detail the role of creep mechanisms in determining the nature of this relationship and from this, the stability of the relationship. It was found that the Monkman–Grant constant depended negatively on the rate of damage accumulation, the initial strain rate, and the rate of hardening, but positively on the strain at failure. It was also found that at 833 K and a high stress, θ_4 was the major determinant of failure times. But as the stress level fell, the parameters θ_3 and θ_1 become more important. The growing importance of θ_3 with decreasing stress implies a bigger role for damage accumulation with decreasing stress (as $\hat{W} = 1/\theta_3$). At the highest stress, the rate of softening was the biggest contributor to variations in failure time but with decreasing stress, damage accumulation and hardening play a bigger role in determining the variation in failure times.

https://doi.org/10.1007/s11661-025-07905-2

I. INTRODUCTION

12Cr–1Mo–V–Nb steel (also referred to as T12 steel or ASTM A387 Grade 12: Class 2 steel) is a type of low-alloy steel that is often classified as a heat-resistant steel. The alloying elements contained within it contribute to its enhanced strength and creep resistance at high temperatures, as well as its good resistance to corrosion and good weldability properties. It is currently used in ultra-super-critical boilers as superheater and reheater tubes that typically operate at temperatures above 873K and stresses exceeding 25 MPa. It is also a material considered for use in advanced nuclear reactors—including fourth-generation nuclear reactors. These reactors typically operate in the range 1025K to 1273K and the range 5 to 10 MPa. Whilst it is not commonly used for critical turbine components like blades or rotors, this steel can be used for the parts of turbines that are exposed to moderate temperatures and stresses where good resistance to creep and oxidation is required.

For the safe operation of such components and systems, a creep rupture life in the time range of 10^5 hours is required. Evaluation of such long-term creep rupture is typically done using accelerated creep tests (either at accelerated stresses and or temperatures), with creep models then being used to extrapolate to the lower stresses observed in the above-mentioned systems. However, there is little agreement on what creep models perform best at this, and whilst some more recently developed models have been shown to perform well at such extrapolation over a wide range of materials, they currently lack the theoretical backing that provides the additional confidence required for widespread use (for example, Yang *et al.*[1] and Wilshire *et al.*[2–6]). An analysis of minimum creep rates *vs*. time to failure—the so-called Monkman–Grant relation[7]—is another suggested way to evaluate long-term creep rupture because once this minimum rate of creep in an on-going creep test is obtained at an early stage of creep, its rupture life is readily evaluated from this relation without a need to extrapolate to a lower stress or temperature.

The Monkman–Grant (MG) relation was first identified using data on the time to failure t_F and the minimum creep rate $\dot{\varepsilon}_m$ both measured from uniaxial creep tests

M. EVANS is with the Institute of Structural Materials, Swansea University Bay Campus, SA1 8EN, Swansea, Wales. Contact e-mail: m.evans@swansea.ac.uk.
Manuscript submitted March 25, 2025; accepted June 30, 2025.

Published online: 25 July 2025

$$t_F = M(\dot{\varepsilon}_m)^{-\rho}, \quad [1]$$

where M (often termed the proportionality constant) has been seen to be material dependent. These authors studied a wide variety of materials and found that the value for ρ was less than, but close to 1. As a result, this relation is often written as

$$t_F = M(\dot{\varepsilon}_m)^{-1}, \quad [2]$$

where M can then be interpreted as the total strain experienced by a specimen if it were crept at a constant strain rate equal to $\dot{\varepsilon}_m$. More recent studies on Nickel-based super alloys and high Chrome steels[8,9] have also found that $0 < \rho < 1$. Abe[9] and Maruyama et. al.[10] also found that in 9Cr steel, $\rho = 1$ over most test conditions, but dropped well below 1 at low stresses. Such deviations from the MG relation of Eq. [2] has been explained in a variety of different ways. Dobes and Milicka[11] suggested that ρ only equals unity in the following modified version of the MG relation and so attributed this deviation to variations in creep strain at failure, ε_F

$$\frac{t_F}{\varepsilon_F} = M(\dot{\varepsilon}_m)^{-1}. \quad [3]$$

Sklenicka and Kucharova[12] found that for 9Cr steel, the value of ρ in Eq. [1] was 0.88, but when Eq. [3] is applied to the data the value for ρ increased to 0.96. In contrast to this, Abe[9] attributed this deviation to accelerating creep strain rates during tertiary creep

$$\frac{\mathrm{d}\ln(\dot{\varepsilon})}{\mathrm{d}\varepsilon} t_F = \left(\frac{t_F}{(t_F - t_m)}\right)(\dot{\varepsilon}_m)^{-1}, \quad [4]$$

where t_m is the time taken to reach the minimum creep rate, ε is the creep strain, and $\dot{\varepsilon}$ the creep strain rate. However, when applied to 9Cr steel, Abe obtained a value for ρ that was still less than 1. Closely related to this modification, Maruyama *et al.*[10] attributed the deviation in 9Cr steel to differences in creep curve shape under low and high stress conditions—they found that the value for ρ differed in four different stress–temperature regimes

These studies suggest that measuring values for $\dot{\varepsilon}_m$ early on, offers little in the way of being able to use this to measure long-term creep rupture. The aim of this paper is therefore to gain some additional insights into this MG relation using data of 12Cr–1Mo–1V–1Nb. More specifically, this paper will derive the MG relation from the 4-θ methodology originally developed by Evans and Wilshire[13] to gain insights into the roles played by creep hardening, softening, and damage mechanisms in determining creep life—and indeed whether these mechanisms also change with test conditions. The paper will therefore quantify the relative importance of these mechanisms in determining times to failure. To achieve these aims the paper is structured as follows. The next section describes the creep tests carried out on this material, and this is followed by a method section outlining how the MG relation can be derived from the 4-θ methodology and how to measure the relative importance of different creep mechanisms in determining creep life within this methodology. These methods are then applied and results presented and discussed. Finally, the conclusion section outlines areas for future work.

II. THE DATA

Thirty-seven cylindrical test pieces were machined from an as-received batch of 12Cr–Mo–V–Nb steel. The chemical composition of this batch of material is shown in Table I. The material was heat treated at 1423K followed by air cooling and then two rounds of 3 hours at 923K (followed by air cooling each time). The tensile strength (σ_{TS}) for this batch of material is 990 MPa at room temperature and 551 MPa at 873K, with corresponding 0.2 pct proof stresses of 831 and 440 MPa.

The specimens were tested in tension over a range of stresses and temperatures using high precision in Andrade–Chalmers constant stress machines at the Interdisciplinary Research Centre (IRC) laboratories at Swansea University. Loads and stresses were applied and maintained to an accuracy of 0.5 pct. In all cases, temperatures were controlled along the gauge lengths and with respect to time to better than ± 1 K. The extensometer could measure tensile strain to better than 10^{-5}. Loading machines, extensometers and thermocouples were all calibrated with respect to NPL traceable standards. The test matrix used for this paper is shown in Table II, where it can be noted that at three different test conditions a replicate test was carried out. Up to 403 creep strain/time readings were taken during each of these tests.

III. METHODOLOGY

A. *An Empirical Representation of the 4-θ methodology*

The 4-θ methodology developed by Evans and Wilshire[13] was initially put forward as a simple empirical relation to relate strain to time under unchanging test conditions (constant stress and temperature)

$$\varepsilon = \theta_1\left(1 - e^{-\theta_2 t}\right) + \theta_3\left(e^{\theta_4 t} - 1\right), \quad [5]$$

where ε is the strain, t is the time, and θ_1 are the four theta parameters that relate strain to time. Their values depend on test conditions. θ_2 and θ_4 are rate parameters, whilst θ_1 and θ_3 are scale parameters—so, for example, the strain obtained by the end of primary creep is given by θ_1. A specimen on test under uniaxial constant stress and temperature will eventually rupture with a failure time t_F and with a strain at rupture of ε_F

$$\varepsilon_F = \theta_1\left(1 - e^{-\theta_2 t_F}\right) + \theta_3\left(e^{\theta_4 t_F} - 1\right) \quad [6]$$

Given that $-\theta_2$ is a small negative number and t_F a large number, $e^{-\theta_2 t_F} \approx 0$ and so

Table I. Chemical Composition (Wt Pct)

Cr	Co	C	Mn	Si	Ni	Mo	Ti	Al	B	V	S	P	Cu
11.2	0.01	0.16	0.74	0.28	0.52	0.51	0.1	0.05	0.008	0.28	0.015	0.022	0.15

Also 0.029 As, 0.065N, 0.29Nb, 0.019Sn and 0.1W. Balance Fe.

Table II. Test Conditions for Each of the 37 Cut Specimens.

Temperature (K)	Stress (MPa)						
813	440	460	480	500	510		
833	340	390	**410**	460	480		
853	310	325	340	350	360	**390**	460
873	270	308	325	**340**	370		
893	230	250	270	290	310	325	340
923	175	200	220	250	280		

One specimen was placed on test at each shown condition, except the conditions highlighted in bold—where two specimens were placed on test.

$$\varepsilon_F \approx \theta_1 + \theta_3\left(e^{\theta_4 t_F} - 1\right) \quad [7]$$

which can be rearranged for the time to failure

$$t_F \approx \frac{1}{\theta_4}\ln\left[\frac{\varepsilon_F - \theta_1 + \theta_3}{\theta_3}\right] = \frac{1}{\theta_4}\ln\left[1 + \frac{\varepsilon_F - \theta_1}{\theta_3}\right]. \quad [8]$$

Whilst not immediately obvious, this is a type of MG relation. To understand this requires relating the θ_1 to creep mechanisms.

B. *A Constitutive Representation of the 4-θ Methodology*

Sometime after the appearance of this empirical model in the literature, Evans[14] outlined the constitutive foundations behind Eq. [5], *i.e.* provided each term in Eq. [5] with a theoretical explanation in terms of the micro-mechanisms governing creep. So, unlike the Wilshire model mentioned above, creep life predictions based on the 4-θ methodology has a foundation based on creep mechanisms. Following the approach taken by Evans[14], internal state variables can be used to explain the form of Eq. [5] using as a starting point the following creep constitutive law for the strain rate $\dot{\varepsilon}$

$$\dot{\varepsilon} = \Phi\left(\sigma, T, \xi_1, \xi_2, \ldots, \xi_\alpha, \ldots, \xi_p\right), \quad [9]$$

where $\dot{\varepsilon}$ is the rate of strain with respect to time, σ is the stress, T is the absolute temperature, ξ_α are the internal state variables which are time dependent, and $\Phi()$ is (an unknown) functional form. Each of these internal variables will have an equation associated with them that describes their evolution during creep. All the ξ_α describe continuum quantities that could be classified as either hardening or softening, static or dynamic, transitory, or permanent. One possible functional form for Eq. [9] is

$$\dot{\varepsilon} = \dot{\varepsilon}_o f(\xi_\alpha), \quad [10]$$

where $\dot{\varepsilon}_o$ is the initial rate of strain occurring for virgin material when placed on test—that will depend on both stress and temperature. So, $f(\xi_\alpha)$ takes on the value one for such material, but thereafter is modified by the creep processes occurring within the grains or grain boundaries. Next assume that $f(\xi_\alpha)$ is a linear function of several of these internal variables

$$\dot{\varepsilon} = \dot{\varepsilon}_o\{1 + (h_1, h_2, \ldots, h_\alpha, \ldots, h_{mh}) + (r_1, r_2, \ldots, r_\alpha, \ldots, r_{mr}) + (w_1, w_2, \ldots, w_\alpha, \ldots, w_{mw})\}, \quad [11]$$

where the h_α, r_α, and w_α are dislocation hardening, dislocation softening, and damage internal variables, respectively. Softening (or recovery) variables are positive in value. Each r_α variable can represent a diverse range of softening mechanism possibly including (but maybe not exclusively so) those associated with climb and glide, the annihilation of mobile dislocations or their rearrangement into sub-boundaries, the formation of precipitates that depletes solid-solution strengthening elements (such as Mo, W, V, Nb) from the grains, recovery of martensite lath boundaries (their evolution into equiaxed grains reducing dislocation density), and the coarsening over time of carbides (like $M_{23}C_6$) and intermetallic phases (*e.g.* Laves phase).

On the other hand, hardening variables are transitory and dynamic in nature and will be negative in value. Each h_α variable can represent a diverse range of hardening mechanism possibly including (but again not exclusively so) the generation of dislocations at a rate faster than they can recover leading to internal resistance that will further limit plastic deformation, dislocations rearranging into organised substructures, such as cells or low-angle boundaries, precipitation of fine MX-type particles (Orowan strengthening), the interaction between dislocations and diffusing solute atoms (*e.g.* N, C), and solid-solution strengthening from the initial alloying elements, such as Mo, W, and V.

The damage variables could include grain boundary sliding, lath martensite recovery and sub grain coarsening, coarsening of $M_{23}C_6$ carbides, alteration in second-phase interfaces, changes in mobile dislocation density and the nucleation of small voids (cavities) at grain boundaries, creep crack nucleation and growth, and oxidation-assisted damage. They are usually dynamic in nature and positive in quantity. More than one of all these processes can occur at a time and each mechanism will be a function of stress and temperature.

As the internal variables in Eq. [11] occur linearly and because Eq. [11] is linear in the coefficients, it is possible

to quantify overall hardening (H), softening (R), and damage (W) through a simple summation

$$H = \sum_{\alpha=1}^{mh} h_\alpha,\ R = \sum_{\alpha=1}^{mr} r_\alpha \text{ and } W = \sum_{\alpha=1}^{mw} w_\alpha. \qquad [12]$$

Evans then postulated the following evolutionary equations for these internal variables:

$$\dot{H} = -\hat{H}\dot{\varepsilon},\ \dot{R} = \hat{R},\ \text{and}\ \dot{W} = \hat{W}\dot{\varepsilon} \qquad [13]$$

where the dot above each variable refers to the rate of change in this variable with respect to time and $\hat{H}$, $\hat{R}$, and $\hat{W}$ are parameter constants found as

$$\hat{H} = \sum_{\alpha=1}^{mh} \hat{h}_\alpha,\ \hat{R} = \sum_{\alpha=1}^{mr} \hat{r}_\alpha \text{ and } \hat{W} = \sum_{\alpha=1}^{mw} \hat{w}_\alpha, \qquad [14]$$

where $\dot{h}_\alpha = -\hat{h}_\alpha\dot{\varepsilon}$, $\dot{w}_\alpha = \hat{w}_\alpha\dot{\varepsilon}$, and $\dot{r}_\alpha = \hat{r}_\alpha$. Eq. [11] can then be written as

$$\dot{\varepsilon} = \dot{\varepsilon}_o(1 + H + R + W). \qquad [15]$$

It is difficult to a obtain a closed form integral of these equations under all situations, but the shape of the normalised creep curves for 12Cr–Mo–V–Nb steel seen in Figure 1 suggests that some approximations can be used—which will not significantly affect the modelling results. It can be seen from this figure that *i*. the duration (in terms of time) of primary creep is very short, ii. most of the creep process consists of secondary creep, and iii. there is slow initial acceleration in creep rates at the start of tertiary creep. These three characteristics suggests that damage processes are insignificant early in life and indeed until later on in tertiary creep.

These characteristics were also observed by Kafexhiu *et al.*[15] for this material. For example, these authors noted that at 600 °C and 150 MPa, primary creep lasts only a few hours, followed by a prolonged secondary stage. Their long-term data (*e.g.* 10,000 + hours) showed secondary and tertiary creep domination. Consequently, the value of W in Eq. [15] remains close to zero for a large proportion on the overall creep time, so that the primary creep strain rate can be modelled as

$$\dot{\varepsilon} = \dot{\varepsilon}_o(1 + H + R) \qquad [16]$$

without any significant loss of accuracy. So, under this approximation (that primary creep occurs over small times in relation to the creep life), Evans[14] has shown that Eqs. [12] through [14] leads to

$$\dot{\varepsilon} = \left[\dot{\varepsilon}_o - \frac{\hat{R}}{\hat{H}}\right] e^{-\hat{H}\dot{\varepsilon}_o t} + \frac{\hat{R}}{\hat{H}} \qquad [17]$$

(see the appendix for details). Eq. [17] states that the initial creep rate of $\dot{\varepsilon}_o$, gives way to a rapidly decreasing creep rate until a steady-state rate of creep equal to $\frac{\hat{R}}{\hat{H}}$ is reached where the rate of hardening is balanced by the rate of recovery, *i.e.* until the minimum or secondary creep rate $\dot{\varepsilon}_m$ is reached. This is a very general specification of primary and secondary creep to which a variety of different creep mechanisms can be attached to it. Without this assumption, (*i.e.* integrating Eq. [15]), Eq. [17] becomes

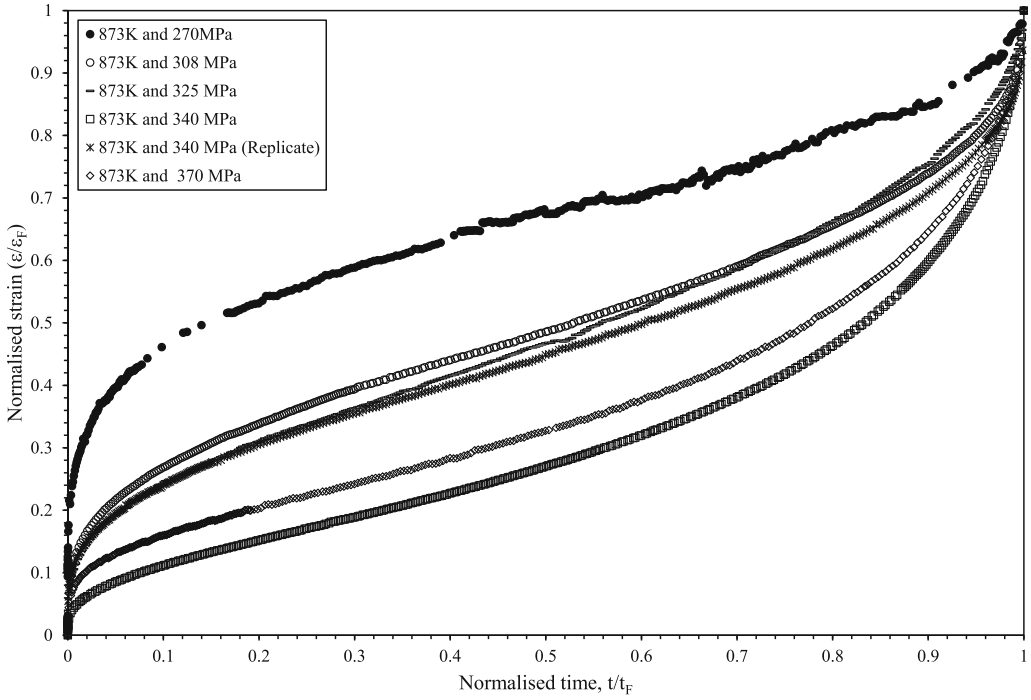

Fig. 1—Normalised creep curves obtained from uniaxial tests carried out at 873 K and various stresses.

$$\dot{\varepsilon} = \left[\dot{\varepsilon}_o + \frac{\hat{R}}{\hat{W}-\hat{H}}\right] e^{-\hat{H}\dot{\varepsilon}_o t} - \frac{\hat{R}}{\hat{W}-\hat{H}} \quad [18]$$

so then the minimum or secondary creep rate is determined by the rate of recovery relative to the excess of the hardening rate over the damage rate $\frac{\hat{R}}{\hat{W}-\hat{H}}$. Then, the secondary creep rate is determined by hardening, softening, and damage rates occurring during primary creep. But for Eq. [18] to have the characteristics of the creep curves in Figure 1, $\left(\hat{W}-\hat{H}\right) < 0$. Then at the start of a creep test ($t = 0$), the rate of strain is given by $\dot{\varepsilon}_o$ (as $e^o = 1$) and subsequently $\dot{\varepsilon}$ will reduce in value until a value of $\frac{\hat{R}}{\left(\hat{W}-\hat{H}\right)}$ is reached. But for this to happen rapidly as presented in Figure 1, $\hat{W}$ must also be very small relative to $\hat{H}$. That is, damage accumulation in minimal during primary creep or $-\frac{\hat{R}}{\left(\hat{W}-\hat{H}\right)}$ approximately equals $\frac{\hat{R}}{\hat{H}}$ and so can replace $\frac{\hat{R}}{\hat{W}-\hat{H}}$ in Eq. [18]. This simplifying assumption does not affect the results latter, all it means is that when referring to the hardening rate we are really referring to hardening net of any primary damage.

In the 4-θ methodology, it is further assumed that tertiary damage processes then influence this steady-state rate of creep

$$\dot{\varepsilon} = \left[\dot{\varepsilon}_o - \frac{\hat{R}}{\hat{H}}\right] e^{-\hat{H}\dot{\varepsilon}_o t} + \frac{\hat{R}}{\hat{H}}[1 + W]. \quad [19]$$

This simplifying approach does not mean that damage is confined to tertiary creep. Instead, it means damage generation is restricted to those strains arising from the secondary creep process, which is present throughout the whole of primary creep. Upon extracting all primary creep

$$\dot{\varepsilon}_T = \frac{\hat{R}}{\hat{H}}[1 + W], \quad [20]$$

where $\dot{\varepsilon}_T$ is the tertiary strain rate. Evans showed that this can be rewritten in terms of time t

$$\dot{\varepsilon}_T = \frac{\hat{R}}{\hat{H}} e^{\frac{\hat{R}}{\hat{H}}\hat{W}t} \quad [21]$$

(also see appendix for this derivation). Substituting this into Eq. [19] gives

$$\dot{\varepsilon} = \left[\dot{\varepsilon}_o - \frac{\hat{R}}{\hat{H}}\right] e^{-\hat{H}\dot{\varepsilon}_o t} + \frac{\hat{R}}{\hat{H}} e^{\widehat{\frac{\hat{W}R}{H}}t} \quad [22]$$

and upon integration

$$\varepsilon = \frac{1}{\hat{H}\dot{\varepsilon}_o}\left[\dot{\varepsilon}_o - \frac{\hat{R}}{\hat{H}}\right]\left(1 - e^{-\hat{H}\dot{\varepsilon}_o t}\right) + \frac{1}{\hat{W}}\left(e^{\widehat{\frac{\hat{W}R}{H}}t} - 1\right). \quad [23]$$

An important advantage of this theta methodology is that all the internal variables can be easily and directly calculated from the θ values describing a uniaxial creep curve. So, comparing Eq. [23] to Eq. [5], it follows that

$$\dot{\varepsilon}_o = \theta_1\theta_2 + \theta_3\theta_4;\ \hat{W} = \frac{1}{\theta_3};\ \hat{H} = \frac{\theta_2}{\dot{\varepsilon}_o};\ \hat{R} = \frac{\theta_2\theta_3\theta_4}{\dot{\varepsilon}_o}. \quad [24]$$

This approach makes it particularly useful for finite element modelling of more complex structures and situations where the stress is multiaxial and continually changing during the deformation process—*e.g.* in modelling the small punch test. Instead of using strain, time or life fraction hardening rules in such models, the estimated theta parameters can be used to recompute H, R, and W, as a result of changes in stress—which in combination with Eq. [15] allows the new point on the new stress creep curve to be quantified.

Equation [24] is another way of showing that the two assumptions made in the derivation of Eqs. [22, 23] do not remove the appearance of damage from primary creep. In Eq. [24] θ_3 determines the rate of damage accumulation $\widehat{W}$. But θ_3 also determines, in part, the values for $\hat{R}$ and $\dot{\varepsilon}_o$ and thus $\hat{H}$ and so it follows that the rate of damage accumulation also controls primary creep. So, the assumptions only restricts damage generation to those strains arising from the secondary process, which is present throughout the whole of primary. It is these assumptions that directly leads to or implies the existence of the well-established Monkman–Grant relationship that relates fracture behaviour to the product of the secondary creep rate and failure time rather than total strain. The next section looks at this in more detail.

C. *4-θ and the Monkman–Grant Relationship*

Equation (24) then allows the failure time relationship of Eq. [8] to be written as

$$t_F \approx \frac{1}{\hat{W}}\ln[1 + W_F]\,(\dot{\varepsilon}_m)^{-1} = M(\dot{\varepsilon}_m)^{-1} = M\left(\frac{\hat{R}}{\hat{H}}\right)^{-1}, \quad [25]$$

where W_F is the damage accumulated at failure and the minimum creep rate $\dot{\varepsilon}_m$ is measured as $\frac{\hat{R}}{\hat{H}}$

$$W_F = \hat{W}(\varepsilon_F - \varepsilon_p), \quad [26]$$

$\varepsilon_p = \theta_1$ is the strain at the end of primary creep. This of course is the familiar Monkman–Grant expression. The 4-θ methodology thus predicts the exponent on $\dot{\varepsilon}_m$ is equal to -1. This theta methodology explains the role of the minimum creep rate in determining failure time through the assumption that damage accumulation works by accelerating the minimum creep rate, thereby leading to strain accumulation that eventually results in failure. The constant M is seen to directly depend on the strain at failure ε_F (but not in the way suggested by Dobes and Milicka[11]) and the rate of damage

accumulation $\hat{W}$. It also depends indirectly on the initial rate $\dot{\varepsilon}_o$ and minimum rate $\dot{\varepsilon}_m$ through ε_p (as θ_1 plays a role in determining $\dot{\varepsilon}_o$) and thus $\hat{R}$ and $\hat{H}$. To the extent to which some or all these variables depend on stress and temperature, the 4-θ methodology casts doubt on the constancy of M and the Monkman–Grant relation over all test conditions.

Equations (25, 26) also suggest that the exact nature on the Monkman–Grant relation depends on the shape of the creep curve, a point recently raised by Maruyama *et al.*[10] for a similar material (9Cr–1Mo steel). However, they used a purely empirical logarithmic creep equation that was not related to any creep mechanism. As such, they were unable to quantify the relative importance of damage, softening, and hardening in determining the time to failure. Reductions in $\hat{W}$ will result in a creep curve with smaller amounts of tertiary strain accumulation and so with all other variables determining M being unchanged, this will lead to a larger time to failure (M will be large because the increase in $1/\hat{W}$ will exceed the reduction in the contribution of $\hat{W}$ to W_F in Eq. [26] due to the log transformation). Likewise, a higher hardening rate will decrease $\dot{\varepsilon}_m$ and so increase the amount of primary strain accumulation but it will also shorten the time taken to reach this minimum rate—*i.e.* will lead to a shorter but well-defined primary phase of the creep curve.

To further illustrate the link between Eqs. [25, 26] and creep curve shape consider a scenario where two creep curves have been obtained (under different test conditions) that have the same values for $\hat{W}, \dot{\varepsilon}_o, \varepsilon_F$ and $\dot{\varepsilon}_m$, but different hardening rates (and so different softening rates given the same $\dot{\varepsilon}_m$).The first specimen in Figure 2(a) has the higher hardening rate and so reaches the same minimum creep rate before specimen 2. Given the same failure strain and the same damage rate, this forces specimen 1 to fail first (t_{F1}) because it reached the minimum creep rate first. Thus, as shown by Eqs. [25, 26], failure time and the hardening rate are negatively related when all other determinants of failure time are the same and unchanging. Likewise in Figure 2(b), the first specimen has the higher damage rate but the same values for $\dot{\varepsilon}_o$, $\hat{H}$, $\hat{R}$, ε_F and $\dot{\varepsilon}_m$ and so reaches the minimum creep rate at the same time as specimen 2. However, the same failure strain forces specimen 1 to fail first (t_{F1}), because the higher damage rate forces strain to accumulate towards ε_F much quicker for specimen 2. Thus, as shown by Eqs. [25, 26] failure time and the damage rate are negatively related when all other determinants of failure time are the same and unchanging.

The remaining sub-sections show how Eqs. [25, 26] can be used to identify the relative importance of hardening, softening and damage accumulation in the determination of the time to failure.

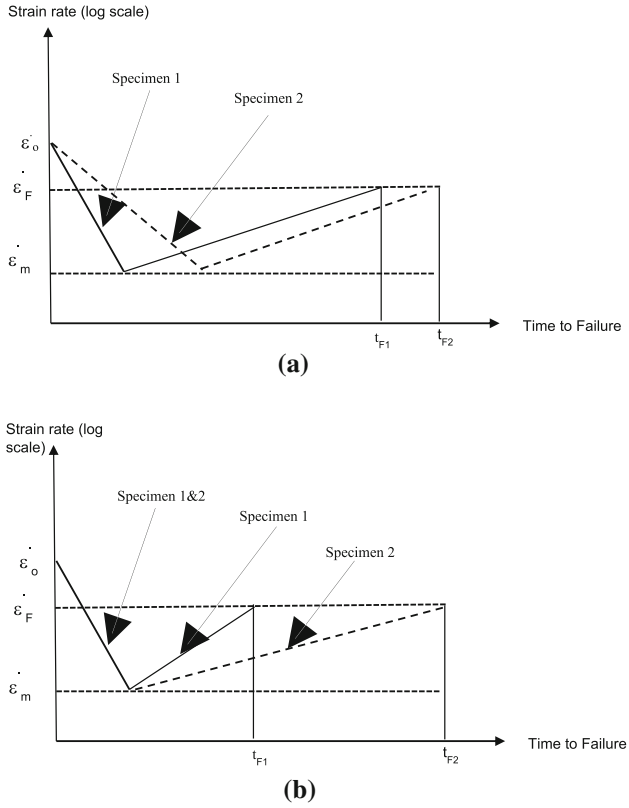

Fig. 2—(*a*) Schematic representation for the creep of two specimens with different hardening rates, but identical values for $\dot{\varepsilon}_o$, ε_F, $\hat{W}$, and $\dot{\varepsilon}_m$. (*b*) Schematic representation for the creep of two specimens with different damage rates but identical values for $\dot{\varepsilon}_o$, $\hat{H}$, $\hat{R}$, ε_F and $\dot{\varepsilon}_m$.

D. *Estimating the* θ_l

Evans[16] developed a non-linear least squares procedure to estimate the θ_l values in Eq. [5] from the strain–time results obtained from a uniaxial creep test carried out at constant stress and temperature. The theta parameters are obtained by iteratively carrying out a series of linear regressions, where the variables in these regressions are a set of derivative variables. Let a measured creep curve obtained at a given temperature and stress be made up of i = 1 to n strain–time pairings. Starting values for the θ_l parameters are first chosen—$\theta_{l,0}$. This enables the residual strain series to be calculated as

$$e_{i,o} = \varepsilon_i - \left\{\theta_{1,0}\left(1 - e^{-\theta_{2,0}t_i}\right) + \theta_{3,0}\left(\theta_{4,0}e^{\theta_{4,0}t_i} - 1\right)\right\}. \quad [27]$$

These starting values can then be used to compute initial values for the analytical first partial derivatives

$$\frac{de_{i,0}}{d\theta_{\ell,0}} \text{ for } \ell = 1,\ 4, \quad [28]$$

where, for example, (l = 2)

$$\frac{de_{i,o}}{d\theta_{2,o}} = -t_i\theta_{1,0}\ e^{-\theta_{2,o}t_i}. \quad [29]$$

A first-order Taylor series approximation to Eq. [27] is given by

$$e_{i,o} \cong (\theta_{1,1} - \theta_{1,0}) \frac{\mathrm{d}e_{i,\mathrm{o}}}{\mathrm{d}\theta_{1,\mathrm{o}}} + \ldots + (\theta_{4,1} - \theta_{4,0}) \frac{de_{i,o}}{d\theta_{4,0}} \quad [30]$$

and so the regression coefficients obtained from a multiple regression of $e_{i,o}$ on all the $\frac{\mathrm{d}e_{i,\mathrm{o}}}{\mathrm{d}\theta_{\ell,\mathrm{o}}}$ will yield updated values for all the theta parameters, *i.e.* $\theta_{1,1}$ is an improved estimate for θ_1 (compared to the starting value $\theta_{1,o}$). $\theta_{1,1}$ to $\theta_{4,1}$ then replace $\theta_{1,0}$ to $\theta_{4,0}$ and the above steps are repeated until convergence is reached—at which point the updated theta estimates are the same as the previous values (or to within a pre-defined small difference).

Necking in not part of tertiary creep and results in a deviation in the creep rates from the 4-θ tertiary rate given by the exponential relation $\theta_3\theta_4 e^{\theta_4 t}$. When the actual rates diverge from this predicted rate, the raw data are truncated back to where the divergence begins. The presented theta parameters in this paper are those obtained from the truncated sample to ensure a more accurate representation of tertiary creep, *i.e.* to prevent necking exaggerating the rate of tertiary creep.

Of course, these are estimates of the true values for each θ_1, which is reflected in the fact that these estimates have a standard error associated with them—so that the larger is this standard error the greater is the possibility that the estimates made for θ_1 using Eq. [30] differs from its true value. Provided these estimates are unbiased, the estimated value can be considered as being equal to the mean value. An estimate of these standard errors is given by the square root of the diagonal elements of the 4x4 covariance matrix **V**

$$\boldsymbol{V} = \mathrm{s}^2 \left(\mathbf{X}^{\mathrm{d}/} \mathbf{X}^{\mathrm{d}} \right)^{-1}. \quad [31]$$

In Eq. [31], $\mathbf{X}^{\mathrm{d}}$ is the n x 4 matrix of the derivative variables in Eq. [30] obtain on the last iteration (say iteration f), so that, for example, the first column of $\mathbf{X}^{\mathrm{d}}$ contains the $i = 1$ to n values on $\frac{de_{i,f}}{d\theta_{1,f}}$. $\mathbf{X}^{\mathrm{d}/}$ is the transpose of $\mathbf{X}^{\mathrm{d}}$ and $s^2 = \sum_{i=1}^{n} \left(e_{i,f}\right)^2/\mathrm{n}$—4. V_{11} is then the value in the first row and column of **V** and so gives the variance for θ_1, whilst V_{44} is the value in the fourth row and column of **V** and so gives the variance for θ_4.

Unfortunately, due to the nature of creep testing, the values for $e_{i,f}$ will be autocorrelated. A typical pattern for this autocorrelation has been shown to take the form:

$$e_{i,f} = \lambda e_{i,f} + v_i, \quad [32]$$

where v_i is a white noise error term and λ is usually very close to 1 in value. The consequence of this phenomenon is that the variance estimates given by V_{II} are deflated in comparison to their true values. This paper uses the Newey–West[17] method (see also Evans[18] for an application of this method to creep of a 1Cr rotor steel) to produce variance estimates that are robust to this autocorrelation and so asymptotically closer to their true values. These procedures are all implemented within Excel.

E. *Computing the Mean and Variances for the Internal Variables*

There are several approaches to determining the mean and variance of a function. One is to use an approximation. Suppose that a variable y is functionally related to k different other variables (x_1 to x_k)

$$y = f(x_1, x_2, \ldots\ldots, x_k). \quad [33]$$

An approximation (based on a first-order Taylor series expansion around the mean) to the mean and variance of this function is given by

$$\overline{y} = f(\overline{x}_1, \overline{x}_2, \ldots\ldots, \overline{x}_k), \quad [34]$$

$$\mathrm{Var}[y] = \mathrm{Var}[x_1] \left[\frac{\mathrm{d}y}{\mathrm{d}x_1}\right]^2 + \mathrm{Var}[x_2] \left[\frac{\mathrm{d}y}{\mathrm{d}x_2}\right]^2 + \ldots\ldots + \mathrm{Var}[x_k] \left[\frac{\mathrm{d}y}{\mathrm{d}x_k}\right]^2, \quad [35]$$

where $\overline{x}_k$ is the mean value for x_k and Var[] stands for the variance of the variable shown in square parenthesis. The squaring of derivatives reflects the fact that variances are always additive. As an example, consider the variance of $\dot{\varepsilon}_{\mathrm{o}} = \theta_1\theta_2 + \theta_3\theta_4$. The variances for each θ_1 are given along the diagonal of the **V** matrix of Eq. [31]—adjusted for autocorrelation—and using these values, the variance for $\dot{\varepsilon}_{\mathrm{o}}$ can be found as

$$\mathrm{Var}[\dot{\varepsilon}_{\mathrm{o}}] = \mathrm{Var}[\theta_1] \left[\frac{\mathrm{d}\dot{\varepsilon}_o}{\mathrm{d}\theta_1}\right]^2 + \mathrm{Var}[\theta_2] \left[\frac{\mathrm{d}\dot{\varepsilon}_o}{\mathrm{d}\theta_2}\right]^2 + \mathrm{Var}[\theta_3] \left[\frac{\mathrm{d}\dot{\varepsilon}_o}{\mathrm{d}\theta_3}\right]^2 + \mathrm{Var}[\theta_4] \left[\frac{\mathrm{d}\dot{\varepsilon}_o}{\mathrm{d}\theta_4}\right]^2, \quad [36]$$

where $\frac{\mathrm{d}\dot{\varepsilon}_o}{\mathrm{d}\theta_1} = \theta_2$, $\frac{\mathrm{d}\dot{\varepsilon}_o}{\mathrm{d}\theta_2} = \theta_1$, $\frac{\mathrm{d}\dot{\varepsilon}_o}{\mathrm{d}\theta_3} = \theta_4$, and $\frac{\mathrm{d}\dot{\varepsilon}_o}{\mathrm{d}\theta_4} = \theta_3$, all of which are evaluated using the estimated (*i.e.* mean) values for each θ_1.

Another approach is to use simulation by assuming a distribution for each θ_1 and then randomly drawing values for each θ_1. The starting point in this procedure is to draw values at random within the range 0 to 1. First, choose an initial "seed" number $\mathrm{X_r}$. Then, perform the following division

$$Y_r = (c + aX_r)/m \quad [37]$$

where a, c, and m are whole numbers stored in and used by the algorithm or random number generator. Some values for these constants produce a better sequence of random numbers than others. Next, split this value for Y_r into an integer part (I_r)—given by the number before the decimal point—and a remainder part (F_r)—given by the numbers after the decimal point. F_r is therefore our first random number between 0 and 1. To get the next seed, X_{r+1}, use the formula:

$$X_{r+1} = (c + aX_r) - mI_r. \quad [38]$$

This process can be repeated p times to get p random values between zero and one. This is an example of a Linear Congruential Generator (LCG), and in Excel, this can be implemented using its Rand() function. This function uses $a = 1.141\text{x}10^9$, $c = 12820163$, $m = 16777216$. There are variations in this approach designed to make the sequences of drawn values behave more randomly from a statistical perspective. The Mersenne Twister developed by Matsumoto and Nishimura[19] has a very long period of numbers $(2^{19937} - 1)$ without any repeating cycles—which is extremely large compared to the LCG. It also produces less correlation between successive values of the drawn numbers and passes more statistical test of randomness. The Mersenne Twister uses a matrix linear recurrence over a finite binary field. It also involves bit-shifting, bit-masking, and other operations like tempering to improve the randomness and the quality of the output. However, and just like an LCG, once the initial seed is known the sequence of drawn numbers are perfectly predictable—hence, all these random number generators produce pseudo random numbers. This paper uses the Mersenne Twister in Excel to generate sequences of random numbers between zero and unity.

Such a randomly selected value can be interpreted as a randomly selected value for a cumulative probability. When using the normal distribution, Rand() can therefore be thought of as randomly selected area under the standard normal distribution (as the total area under this distribution equals 1), and the Z Table (found at the back of any decent statistics textbook) can then be used to find the corresponding standardised Z value, where Z is defined as

$$Z_\ell = (\theta_\ell - \text{mean value for } \theta_\ell)/\text{Var}[\theta_\ell]^{0.5}. \quad [39]$$

This can be automated in Excel using the formula Normsinv(), where Normsinv() looks up the Z value in the Z table associated with a given area under the standard normal curve, *i.e.* associated with a number between 0 and 1 (that is entered into the empty brackets). It follows from this that a randomly drawn value for each θ_l can be obtained in Excel, when using an LCG, as follows:

$$\text{Mean value for } \theta_\ell + (\text{Var}[\theta_\ell]^{0.5})\ \text{Normsinv(Rand())}. \quad [40]$$

If r values (where r is relatively large) for each θ_ℓ are drawn in this way, the variance of $\dot{\varepsilon}_o$ can be found by inserting these r values for each θ_ℓ into $\dot{\varepsilon}_o = \theta_1\theta_2 + \theta_3\theta_4$. Then, the variance in these r values for $\dot{\varepsilon}_o$ provides an estimate of Var[$\dot{\varepsilon}_o$]

$$\text{Var}\,[\dot{\varepsilon}_o] = \frac{\sum_{i=1}^{r}\left(\dot{\varepsilon}_{o,i} - \bar{\dot{\varepsilon}}_o\right)^2}{r-1};\ \bar{\dot{\varepsilon}}_o = \frac{\sum_{i=1}^{r}\dot{\varepsilon}_{o,i}}{r}. \quad [41]$$

The same technique can be used for the other internal variables.

F. *Measuring Contributions of the Internal Variables to the Recorded Failure Time*

A particular test condition is selected and $i = 1$ to r values for θ_1 to θ_4 for this condition are drawn from independent normal distributions with their means and their standard deviations calculated using the approach outlined in sub-section D above. These r values for θ_1 to θ_4 are then inserted into [24] to obtained r values for $\dot{\varepsilon}_o$, $\hat{H}$, $\hat{R}$, and $\hat{W}$. All these values can be inserted into either Eqs. [8] or Eqs. [25, 26] together with the ε_F value for this test condition, to obtain the r corresponding values for t_F—so yielding a distribution of failure times at that test condition. The resulting distributions for t_F, $\dot{\varepsilon}_o$, $\hat{H}$, $\hat{R}$, and $\hat{W}$ will not necessarily be normally distributed, as it is only linear combinations of normally distributed variates that are also normally distributed.

As all these variables have different units of measurement, they need to be standardised by subtracting the mean and dividing the result by the standard deviation for the variables. Consequently, when a variable takes on a value equal to its mean plus 1 standard deviation, its standardised value equals + 1. Let z stand for such a standardised variable, with a subscript indicating the variable being standardised. For example, the $i = 1$ to r standardised failure times are given by

$$z_{t_{F,i}} = \frac{t_{F,i} - \bar{t}_F}{\sigma_{t_F}}, \quad [42]$$

where $\bar{t}_F$ is the average of the r failure times and σ_{t_F} is the standard deviation in the r failure times. The other standardised variables are thus $z_{\dot{\varepsilon}_{o,i}}$, $z_{\hat{H},i}$, $z_{\hat{R},i}$, $z_{\hat{W},i}$ and $z_{\theta_{\ell,i}}$(for l = 1,4). These standardised variables can then be used in two different ways to measure their contributions to time to failure. First, the r values for $z_{t_{F,i}}$ can be regressed on the r values for one of the variables

$$z_{t_{F,i}} = \beta_1 z_{\theta_{\ell,i}} + \eta_{1,i} \quad [43]$$

when studying the contribution of θ_1 to time to failure or

$$z_{t_{F,i}} = \alpha_1 z_{\dot{\varepsilon}_{o,i}} + \psi_{1,i} \quad [44]$$

when studying the contribution of the initial creep rate to failure time. Here, $\eta_{1,i}$ is the residual or unexplained component of the standardised time to failure—the square of which, when summed over all r values, is minimised in the selection of the value for β_1. Similarly, $\Psi_{1,i}$ is the residual or unexplained component of the standardised time to failure—the square of which, when summed over all r values, is minimised in the selection of the value for α_1. Following a one standard deviation change in the value for θ_l the resulting change in the time to failure, expressed as percentage of one standard deviation in the time to failure, is given by the value for β_1. Similarly, a one standard deviation change in the value for $\dot{\varepsilon}_{o,i}$ produces a change in the time to failure, expressed as percentage of one standard deviation in the time to failure, equal to the value for α_1. The coefficients of determination

associated with Eqs. [43, 44] are defined, respectively, as

$$R^2_{\theta_1} = 1 - \frac{\sum_{i=1}^{r}\left(\eta_{1,i}\right)^2}{\sum_{i=1}^{r}\left(z_{t_{F,i}}\right)^2};\; R^2_{\dot{\varepsilon}_o} = 1 - \frac{\sum_{i=1}^{r}\left(\psi_{1,i}\right)^2}{\sum_{i=1}^{r}\left(z_{t_{F,i}}\right)^2}. \quad [45]$$

As such, $R^2_{\theta_1}$ measures the variation in the standardised t_F values (denominator in Eq. [45]) accounted for by the variation in the standardised values for θ_1 and $R^2_{\dot{\varepsilon}_o}$ measures the variation in the standardised t_F values accounted for by the variation in the standardised values for $\dot{\varepsilon}_o$. Then, in Eq. [43], $z_{\theta_{1,i}}$ is replaced by $z_{\theta_{2,i}}$ and in Eq. [44] $z_{\varepsilon_{0,i}}$ is replaced by $z_{\hat{H},i}$ to obtain values for β_2 and α_2 and the coefficients of determination $R^2_{\theta_2}$ and $R^2_{\hat{H}}$. $R^2_{\theta_2}$ measures the variation in the standardised t_F accounted for by variations in the standardised values for θ_2 and $R^2_{\hat{H}}$ measures the variation in the standardised t_F accounted for by variations in the standardised values for $\hat{H}$. This process is repeated another two times to get the coefficients of determination $R^2_{\theta_3}, R^2_{\theta_4}$ and $R^2_{\hat{R}}, R^2_{\hat{W}}$ and parameters α_3, α_4, β_3, and β_4. Standardising variables ensures that the variables associated with the largest α or β values (in absolute terms) are the bigger contributors to failure time variation. This approach will be referred to as method 1 in the results section.

Instead of performing these sequences of ordinary regressions (regressions containing a single right hand side variable), a series of multiple regressions can be carried out. Here, another of the standardised theta values is added (rather than replacing) to Eq. [43], say $z_{\theta_{2,i}}$

$$z_{t_{F,i}} = \beta^*_1 z_{\theta_{1,i}} + \beta^*_2 z_{\theta_{2,i}} + \eta_{2,i} \quad [46]$$

or another internal variable is added (rather than replacing) to Eq. [44], say $z_{\hat{H},i}$

$$z_{t_{F,i}} = \alpha^*_1 z_{\varepsilon_{0,i}} + \alpha^*_2 z_{\hat{H},i} + \psi_{2,i}. \quad [47]$$

The coefficients of determination associated with Eqs. [46, 47] are defined as

$$R^2_{\theta_{1,2}} = 1 - \frac{\sum_{i=1}^{r}\left(\eta_{2,i}\right)^2}{\sum_{i=1}^{r}\left(z_{t_{F,i}}\right)^2} * \text{ and } R^2_{\dot{\varepsilon}_o,\hat{H}} = 1 - \frac{\sum_{i=1}^{r}\left(\psi_{2,i}\right)^2}{\sum_{i=1}^{r}\left(z_{t_{F,i}}\right)^2}. \quad [48]$$

$R^2_{\theta_{1,2}}$ measures the contribution of θ_1 and θ_2 to the variation in failure times and $R^2_{\dot{\varepsilon}_o,\hat{H}}$ measures the contribution of $\dot{\varepsilon}_o$ and $\hat{H}$ to the variation in failure times. The contributions from just θ_2 or just $\hat{H}$ can then be calculated as

$$R^{*2}_{\theta_2} = R^2_{\theta_{1,2}} - R^2_{\theta_1} \text{ and } R^{*2}_{\hat{H}} = R^2_{\dot{\varepsilon}_o,\hat{H}} - R^2_{\dot{\varepsilon}_o,}. \quad [49]$$

This process can be repeated until all the standardised values are included in the regression:

$$z_{t_{F,i}} = \beta^*_1 z_{\theta_{1,i}} + \beta^*_2 z_{\theta_{2,i}} + \beta^*_3 z_{\theta_{3,i}} + \beta^*_4 z_{\theta_{4,i}} + \eta_{4,i}, \quad [50]$$

$$z_{t_{F,i}} = \alpha^*_1 z_{\varepsilon_{0,i}} + \alpha^*_2 z_{\hat{H},i} + \alpha^*_3 z_{\hat{R},i} + \alpha^*_4 z_{\hat{W},i} + \psi_{4,i}. \quad [51]$$

The coefficient of determination associated with Eqs. [50, 51] are defined as

$$R^2_1 = 1 - \frac{\sum_{i=1}^{r}\left(\eta_{4,i}\right)^2}{\sum_{i=1}^{r}\left(z_{t_{F,i}}\right)^2} \text{ or } R^2_2 = 1 - \frac{\sum_{i=1}^{r}\left(\psi_{4,i}\right)^2}{\sum_{i=1}^{r}\left(z_{t_{F,i}}\right)^2} \quad [52]$$

and the variation in the standardised t_F accounted for by the standardised values for θ_4 or $\widehat{W}$ are given by

$$R^{*2}_{\theta_4} = R^2_1 - R^2_{\theta_{1,2,3}}\; R^{*2}_{\hat{W}} = R^2_2 - R^2_{\dot{\varepsilon}_o,\hat{H},\hat{R}}, \quad [53]$$

where R^2_2 is the variation in standardised failure times explained by the variation in all the internal variable rate parameters and R^2_1 is the variation in standardised failure times explained by the variation in all the theta parameters. This approach will be called method 2 in the results section

Which method is appropriate depends on the nature of all the right-hand side variables in Eqs. [50, 51]. By constructions $z_{\theta_{1,i}}$ to $z_{\theta_{4,i}}$ are all independent of each other, *i.e.* are orthogonal. When this is the case, the two approaches just outlined produce the same results, that is, β^*_1 to β^*_4 equals β_1 to β_4 and more importantly, $R^2_{\theta_1}$ to $R^2_{\theta_4}$ equal $R^{*2}_{\theta_1}$ to $R^{*2}_{\theta_4}$. Either method can be used to measure the importance of the theta values in determining failure times.

However, the r values for the internal variables are not orthogonal by construction. For example, Eq. [24] shows clearly that $\hat{W}$ and $\hat{R}$, both depend on θ_3 and so are bound to be correlated with each other to some degree. This so-called multicollinearity between the right-hand side variables in Eq. [51] means that either method just described suffers from complications. When variables $z_{\varepsilon_{0,i}}, z_{\hat{H},i}, z_{\varepsilon_{\hat{R},i}}, z_{\hat{W},i}$ are correlated with each other, it is possible for $R^2_{\dot{\varepsilon}_o} + R^2_{\hat{H}} + R^2_{\hat{R}} + R^2_{\hat{W}} > 100$ pct, which makes no physical sense. In this situation the first method discussed above cannot be used to measure contributions. Also, when variables $z_{\varepsilon_{0,i}}, z_{\hat{H},i}, z_{\varepsilon_{\hat{R},i}}, z_{\hat{W},i}$ are correlated it is possible for α_1 to α_4 to differ from α^*_1 to α^*_4. This makes it difficult to determine the relative importance of the internal variables in determining failure times based on the values for each α, because it's not clear whether α or α^* is the more accurate estimate of parameter importance.

On the one hand, using just one right-hand variable at a time results in a bias due to the omission of the other variables from the equation, *i.e.* each α value is estimated with systematic error. Whether this bias is upwards or downwards depends on whether the omitted variable is positively or negatively related to the included variable. The absolute bias is larger the greater the correlation between the included and omitted variable. On the other hand, carrying out the multiple regression can also lead to the α^*_1 to α^*_4 being inaccurate

because it becomes impossible to isolate, say, the effects of $z_{\dot{\varepsilon}_{\hat{R},i}}$ and $z_{\hat{W},i}$ on failure times because $z_{\dot{\varepsilon}_{\hat{R},i}}$ and $z_{\hat{W},i}$ themselves vary together. In this example, it is unclear whether the value for α^*_4 measures the effect of the softening or the damage rate on failure times or more likely a combination of both. Nor can we rely on $R^{*2}_{\dot{\varepsilon}_o}, R^{*2}_{H}, R^{*2}_{\hat{R}}, R^{*2}_{\hat{W}}$ to measure importance when multicollinearity is present because then $R^{*2}_{\dot{\varepsilon}_o} + R^{*2}_{H} + R^{*2}_{\hat{R}} + R^{*2}_{\hat{W}} \neq R^2_2$. This is because the value obtained for say $R^{*2}_{\hat{W}}$ depends on the order in which say $z_{\hat{W},i}$ is inserted into Eq. [51]. Adding it before or after another important variable (*e.g.* before or after variable $z_{\hat{R},i}$) will make a big difference to the value obtained for $R^{*2}_{\hat{W}}$—with it being much bigger if added first.

In such circumstances, the best that can be done is to calculate the joint contribution of two or more internal variables to the variation in failure times—the individual values are inseparable due to the correlation between these two or more internal variables. For example, $R^2_{\hat{W}}$ could be calculated as say 92 pct and $R^2_{\hat{R}}$ at say 5 pct when $\hat{W}$ is added to the regression before $\hat{R}$, but at say 4 and 88 pct, respectively, when $\hat{W}$ is added to the regression after $\hat{R}$. This type of result would only occur when $\hat{W}$ and $\hat{R}$ are not orthogonal. This type of result cannot be interpreted as saying $\hat{R}$ is much less important than $\hat{W}$ or visa versa, because a lot of the variation in $\hat{R}$ in these circumstances is picked up in the variation for $\hat{W}$. The more correct interpretation is that somewhere between 88 and 92 pct of the variation in failure times is explained by variations in both $\hat{W}$ and $\hat{R}$. So, when the ordering of variables being added to the regression affects the values for $R^2_{\dot{\varepsilon}_o}, R^2_{H}, R^2_{\hat{R}}$ and $R^2_{\hat{W}}$, multicollinearity is revealing itself as being a problem. Surprisingly, there is no clear link between the degree of multicollinearity and the breakdown of this decomposition of R^2. It can occur even when the correlation between say $\hat{W}$ and $\hat{R}$ is small and it can also be non-existent or minor in magnitude even when this correlation is high.

IV. RESULTS

A. *Estimated Values for the Internal State Variables*

Figure 3(a) shows the estimates made for the initial creep rate upon loading at each test condition, together with the weighted iso-thermal best fit lines. The weights used in obtaining these best fit lines are the inverses of the values given in Figure 3(b) where the ratio of each initial creep rate to its standard deviation are plotted. Irrespective of the temperature, there is a tendency for the initial creep rate to increase with the level of stress. The changing slope of the best fit line reveals quite a complicated relationship between temperature and the initial creep rate—temperature appears to not only shift the best fit line but rotate it in an ill-defined way as well (but generally becoming flatter with increasing temperature). Typically, the standard deviation associated with each initial creep rate is around 10 pct of the estimated value, but at 923 K and 873 K, two of the initial creep rate estimates are very unreliable and at 853 K one initial creep rate estimate is unreliable as revealed by very high ratios in Figure 3(b). Indeed, these ratios are so high, and all the others so similar in magnitude, that the weighted least squares procedure is almost equivalent to removing these initial creep rates from an unweighted best fit line calculation.

Figure 4(a) shows the estimates made for the hardening rate at each test condition, together with the weighted iso-thermal best fit lines. The weights used are the inverses of the values given in Figure 4(b) where the ratio of each hardening rate to its standard deviation are plotted. Irrespective of temperature, decreasing stress tends to lead to an increase in the rate of hardening, as so other things being equal, to a lower minimum creep rate and a smaller reduction in the creep rate as time progresses during tertiary creep. Typically, the standard deviation associated with each hardening rate is around 1 pct of the estimated value, but at 873 K, two of the hardening rate estimates are very unreliable and at 853 K one hardening rate estimate is unreliable as revealed by very high ratios in Figure 4(b). These three data points therefore play a small role in the determination of the shape of the weighted best fit lines.

Figure 4(a) reveals that hardening rates decline with increases in both stress and temperature. Han *et al.*[20] found that in 12Cr–1Mo–V–Nb steels, increased stress and temperature accelerate the coarsening of MX precipitates, leading to a decrease in the material's resistance to creep deformation. This coarsening reduces the effectiveness of precipitate strengthening, resulting in lower creep hardening rates. Higher stresses and temperatures can lead to the annihilation of dislocations, reducing the dislocation density. Since dislocations contribute to work hardening, their reduction leads to a decrease in the material's ability to harden during creep deformation. Since dislocations contribute to work hardening, their reduction leads to a decrease in the material's ability to harden during creep deformation.

Figure 5(a) shows the estimates made for the softening rate at each test condition, together with the weighted iso-thermal best fit lines. Figure 5(b) plots the ratio of each softening rate to its standard deviation. Unlike for the hardening and the initial creep rates, the effect of an increase in stress at a given temperature is to increase the softening rate. Broadly speaking, temperature tends to shift these iso-thermal best fit lines in a parallel fashion. The exception to this is at 893K—but the weights are such that only three data points play a significant role in positioning this iso-thermal line (and so its slope is subject to more uncertainty). Typically, the standard deviation associated with each softening rate is between 1 and 10 pct of the estimated value, but there are around five softening rates whose standard deviation is equal to or more than the actual estimated value.

Figure 5(a) shows that softening rates increase with stress at this temperature. Several studies on this material have also observed this phenomenon. The study by Pešička[21] found for this alloy that during

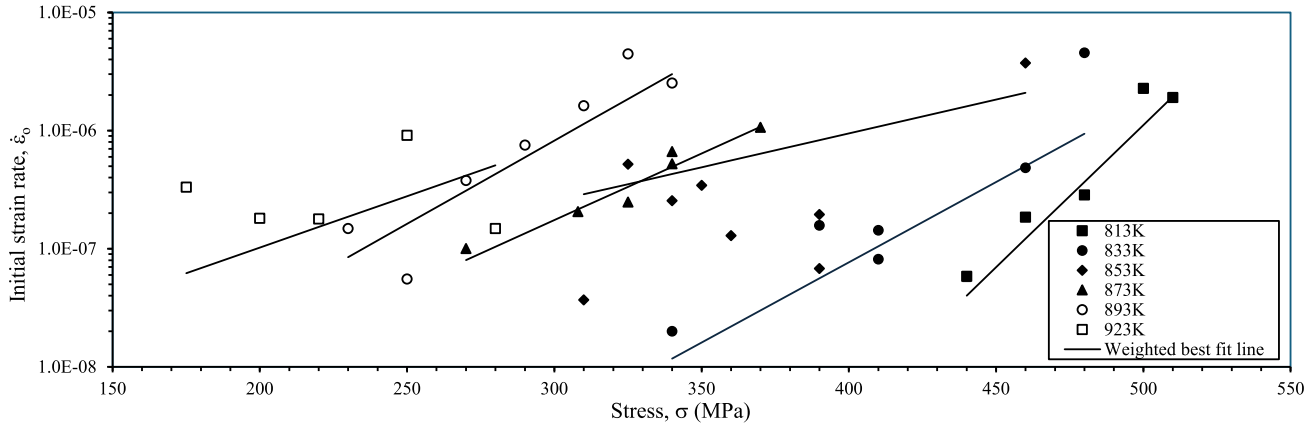

(a)

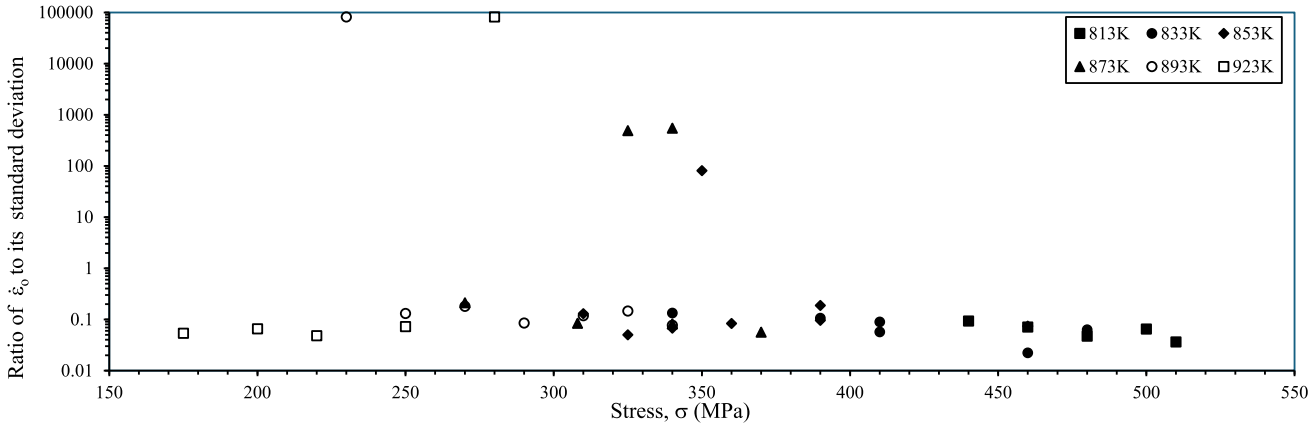

(b)

Fig. 3—Variation of (*a*) the estimates made for the initial creep rate with each test condition together with the weighted iso-thermal best fit lines, and (*b*) the variation of the ratio of these estimates to their standard deviation with test conditions.

creep at 923K, the mean subgrain size increased under both high and low initial stress levels. Notably, carbide particle coarsening was more pronounced at the lower stress level, suggesting that higher stresses can accelerate softening processes. Further, a study by Dudova[22] indicated that the evolution of lath width during creep depends on the stability of precipitates located on the lath boundaries. The study found that a sharp increase in lath width or subgrain size above 1 μm usually corresponds to the transformation of the lath structure into a sub grain structure, which is more likely to occur under higher stress conditions. These studies underscore the complex interplay between stress, temperature, and microstructural evolution in these materials.

Several damage mechanisms have been identified for 9-12Cr steels. Parker[23] identified the nucleation of voids at precipitates and inclusions followed by growth and coalescence as a major damage mechanism—with void nucleation being influenced by the size and distribution of these precipitates and stress conditions. Pešička *et al.*[21] found that 12 pct Cr steels exposed to service conditions displayed subgrain growth and precipitate coarsening—specifically the coarsening of precipitates like $M_{23}C_6$ and Laves phases. Void formation was particularly prevalent at high temperatures and moderate to high stresses, whilst coarsening and grain boundary sliding was confined to high temperatures with stress having only an indirect influence.

Figure 6(a) shows the estimates made for the damage rate at each test condition, together with the weighted best fit iso-thermal lines. Figure 5(b) plots the ratio of each damage rate to its standard deviation are plotted. Unlike the hardening and softening rates, the damage rate does not appear to have any clear relationship with either stress or temperature. Although the figure plots the best fit lines, a possible interpretation of Figure 6(a) is that the damage rate is broadly independent of both stress and temperature, but that there are two broadly distinct levels. The first level corresponds to low damage rates of between 1 and 10 occurring mainly at the lowest recorded stresses and at the highest temperatures. This is consistent with the work carried out by Pešička *et al.*[21] who found void formation required at least moderate stresses. The higher damage rates observed at the largest temperature of 923K is also consistent with the work by Parker[23] who found nucleation of voids and coarsening was bigger at higher temperatures. Pešička *et al.*[21] also found that coarsening was more prevalent at higher

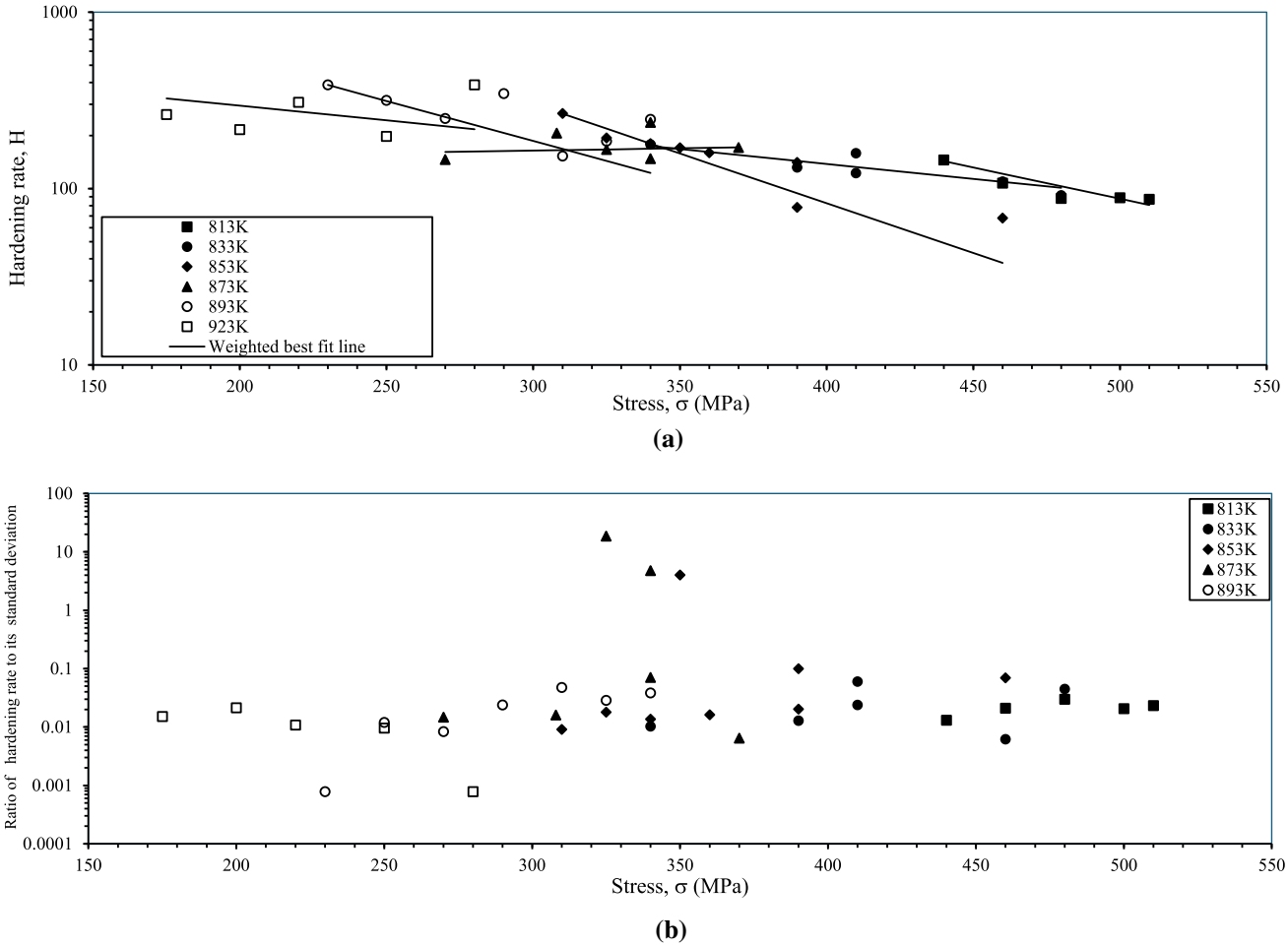

Fig. 4—Variation of (*a*) the estimates made for the hardening rate with each test condition together with the weighted best fit iso-thermal lines, and (*b*) the variation of the ratio of these estimates to their standard deviation with test conditions.

stresses—hence, the relatively large values for the damage rate at the highest stresses in Figure 6(a).

Figure 7 shows the variation of strain at failure with stress and temperature, together with unweighted iso-thermal best fit lines. Apart from at the very highest temperatures, there appears to be a positive relationship between failure strain and stress. The relationship between failure time and temperature is less clear, with temperature changing both the slope and intercept of the best fit iso-thermal lines. The figure also reveals that at an unchanging test condition, there can be substantial variability in the measured failure strain. For example, at 853K and 390 MPa, two specimens were put on test and the strain at failure varied from 4.2 to 6.8 pct. Then at 833K and 410 MPa, two specimens were also put on test and the strain at failure varied from 3.3 to 4.8 pct. The variability 873K and 340 MPa is similar (3.1 to 1.7 pct).

What Figures 3, 4, 5, 6, and 7 suggest about the changing shape of a creep curve with respect to test conditions is revealed in Figure 8 where the variation in the strain rate with time is shown at 833 K over four different stress levels (from the largest to smallest stress used at this temperature). The first thing to note is that as the stress decreases, the hardening rate increases and the softening rate decreases. As a result, the minimum creep rate decreases with increasing stress as clearly seen in this figure. The other effect of these changing rate values is that the strain at the end of primary creep (ε_P) diminishes with stress—with more rapid hardening comes a greater and more rapid reduction in the strain rate compared to the initial rate and this effect is amplified by a lower rate of softening which prevents dislocations from overcoming the barriers to movement. This all results in a much shorter period of primary creep with decreasing stress.

Figure 8 also reveals a reduction in the rate of damage accumulation with stress. Indeed, at the lowest stress, the damage rate is close to zero, so that after primary creep there is a long period of secondary creep (and virtually no tertiary creep) leading to failure. The variation in damage at failure (W_F—see Eq. [26]) with stress is a little less clear from this figure. As can be seen from Figure 8, the value for ε_F and ε_P decreases with stress, but $\hat{W}$ firstly increases with decreasing stress but then decreases with further decreases in stress. The fall in ε_P was explained above in terms of the changes in hardening and softening rates. The consequence of all

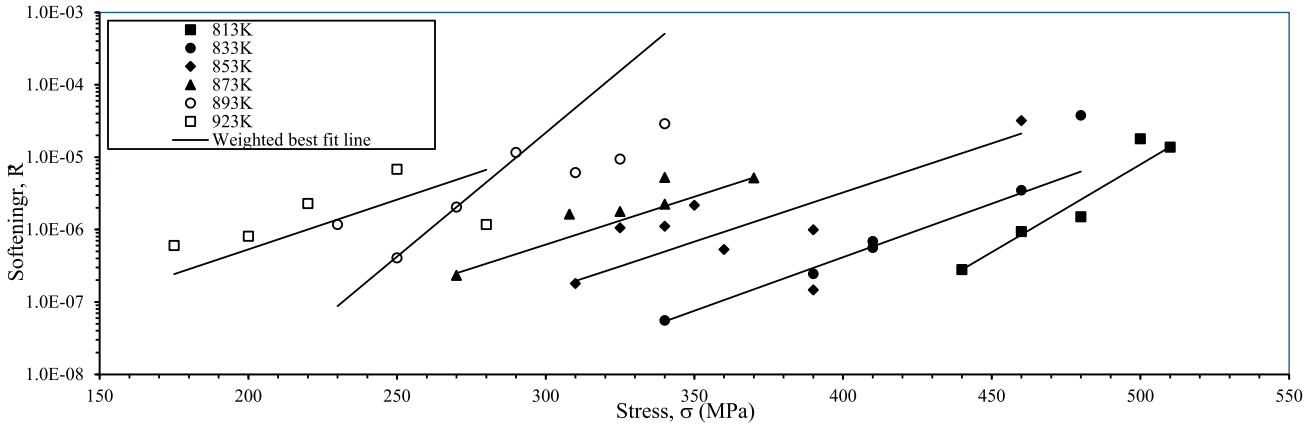

(a)

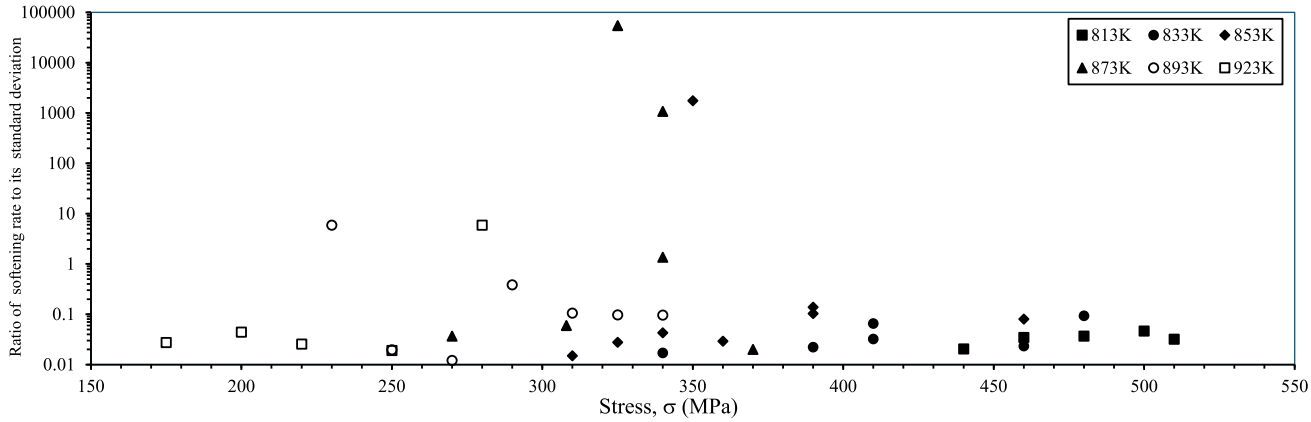

(b)

Fig. 5—Variation of (*a*) the estimates made for the softening rate with each test condition together with the weighted best fit iso-thermal lines, and (*b*) the variation of the ratio of these estimates to their standard deviation with test conditions.

this is that W_F falls dramatically as the stress falls from 460 to 410 MPa even though $\hat{W}$ is roughly the same at these two stresses. This occurs because of a narrowing of the gap between failure strain and primary creep strain which is the result of ε_F failing faster than ε_P between these two stresses (with the fall in ε_P governed by the changes in hardening and softening rates). The rapid fall in ε_F may just reflect the large variability present in rupture strain data—for example, if the rupture strain (of 6.2 pct) associated with the repeat creep curve at 410 MPa is used in Eq. [26], W_F rise to 8.1.

The fit to the data obtained using the 4-θ methodology is also seen in Figure 8. In all four tests conditions the fit to the actual primary and secondary creep rates is very good. The fit appears to be less good for tertiary creep, but this reflects the estimation procedure discussed earlier. Recall that necking in not part of tertiary creep and results in a deviation in the creep rate from the 4-θ tertiary rate given by the exponential relation $\theta_3\theta_4 e^{\theta_4 t}$. When the actual rates diverge from this predicted rate, they are not used in estimating the theta parameter values. As such, the fits shown in Figure 8 show pure tertiary creep, and the gap between this modelled tertiary creep rate and the actual rates is then attributable to necking.

B. *Decomposition of the Time to Failure at 833K and 480 MPa with Fixed Failure Strain*

Figure 9 plots some 2500 generated failure times at 833K and 480 MPa as a frequency histogram, where the vertical axis is scaled so that the area of all the bars sums to 1 (and in all the other histograms contained in this paper). The mean of these failure times was 62,109 seconds (17.25 hours) with a standard deviation of 4657 seconds (1.29 hours). There is a slight skew in this distribution to the right (despite the θ values being treated as normally distributed) and the actual time to failure recorded at this condition is a little above the mean of the distribution. Despite the small size of the standard errors for the theta parameters at this test condition, this transmits into quite a large variation in the times to failure around the mean.

Figure 10(a) shows the contribution of each θ parameter to the variation in times to failure using method 1. At this relatively high stress, most of the variation in failure times shown in Figure 9 is explained

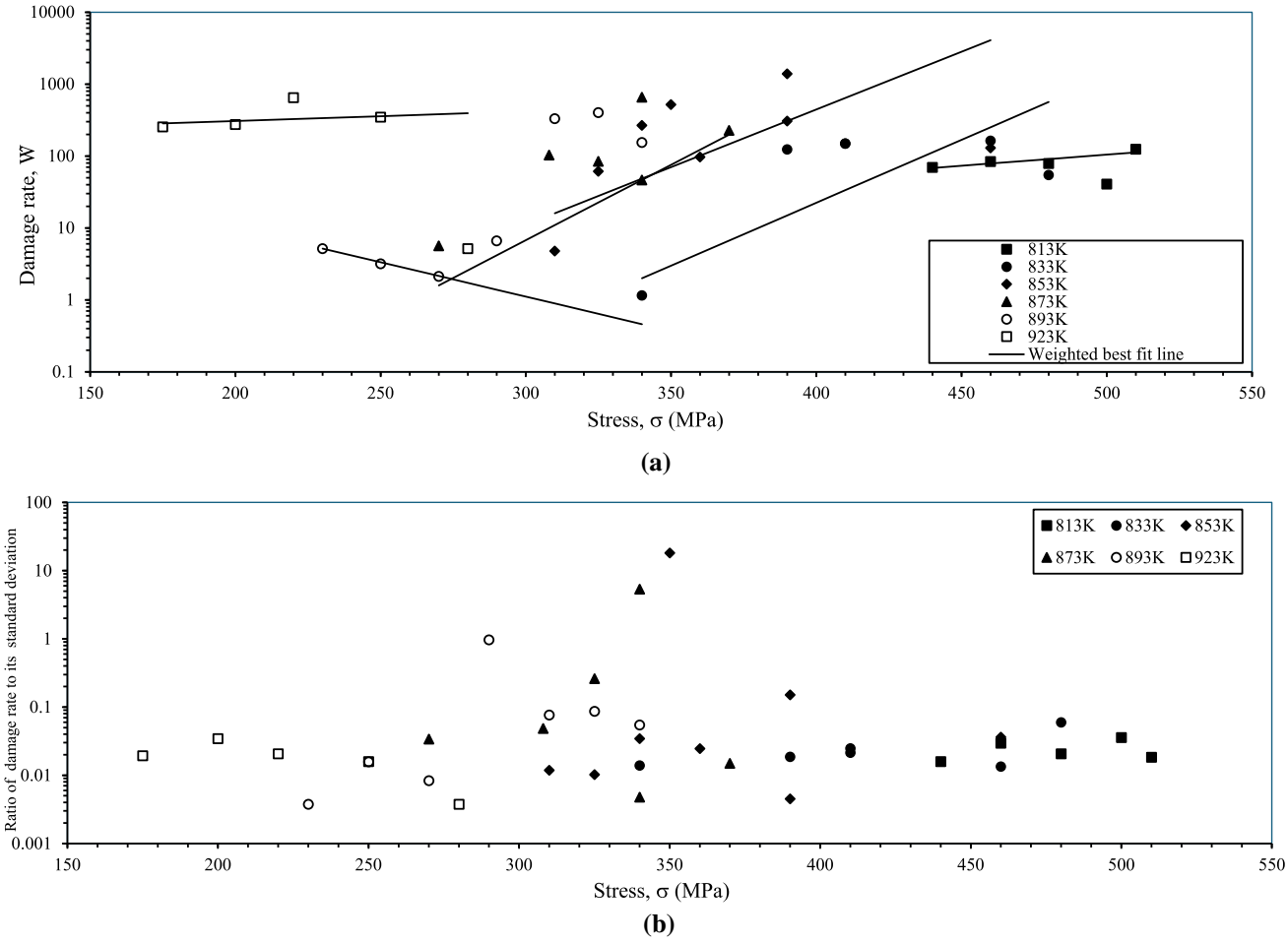

Fig. 6—Variation of (*a*) the estimates made for the damage rate with each test condition together with the weighted best fit iso-thermal lines, and (*b*) the variation of the ratio of these estimates to their standard deviation with test conditions.

by the uncertainty associated with θ_4—just over 80 pct. Much of the remaining variation in times to failure is accounted for by the uncertainty associated with the estimate for θ_3—approximately 17.4 pct. This then translates into the contributions shown in Figure 10(b) obtained using method 1, where around 63.6 pct of the variation in failure times is due to softening during primary creep, with only 17.3 pct of the variation in failure times being the result of damage processes during tertiary creep.

This result is further confirmed in Figure 11 where each internal rate parameter is cross plotted against failure times and the R^2 values shown in this figure are the same as those in Figure 10(b). The best fit line in Figure 10(a) reveals that a 1 standard deviation increase in the hardening rate (equivalent to a change of 4.16 units) leads to an increase in failure times equal to 26.6 pct of the standard deviation in failure times—equivalent to 1240 seconds (or 0.34 hours). In comparison to this, Figure 11(b) reveals that a 1 standard deviation increase in the softening rate (equivalent to a change of 3.48×10^{-6} units) leads to a decrease in failure times equal to 79.8 pct of the standard deviation in failure times—or 3719 seconds (1.03 hours). This a much larger effect compared to the effect of changes in hardening. The effect of changes in the damage rate is in between these two extremes. The best fit line in Figure 11(c) reveals that a 1 standard deviation increase in the damage rate (equivalent to a change of 3.26 units) leads to an increase in failure times equal to 41.6 pct of the standard deviation in failure times—equivalent to 1939 seconds or (0.54 hours). Figure 11(d) shows that changes in the initial strain rate has the smallest impact of failure times.

A note of caution is required however as $\hat{W}$ and $\hat{R}$ are strongly correlated with a correlation coefficient of -0.6. This is not surprising as Eq. [24] shows clearly that $\hat{W}$ and $\hat{R}$, both depend on θ_3 and so are bound to be correlated with each other to some degree. This so-called multicollinearity between the right-hand side variables in Eq. [51] means that both methods 1 and 2 suffer from complications. This reveals itself in differences in the contributions measured by each method. Each method produces similar failure time contributions from $\dot{\varepsilon}_o$ and $\hat{H}$. However, method 2 yielded $R^{*2}_{\hat{R}} = 83.9$ pct and $R^{*2}_{\hat{W}} = 7.4$ pct when $\hat{R}$ is added to Eq. [51] before $\hat{W}$. This differs from the values obtained using method 1 [as seen in Figure 10(b)] where $R^2_{\hat{R}} = 63.6$ pct and $R^2_{\hat{W}} = 17.3$ pct. Given the impact of multicollinearity,

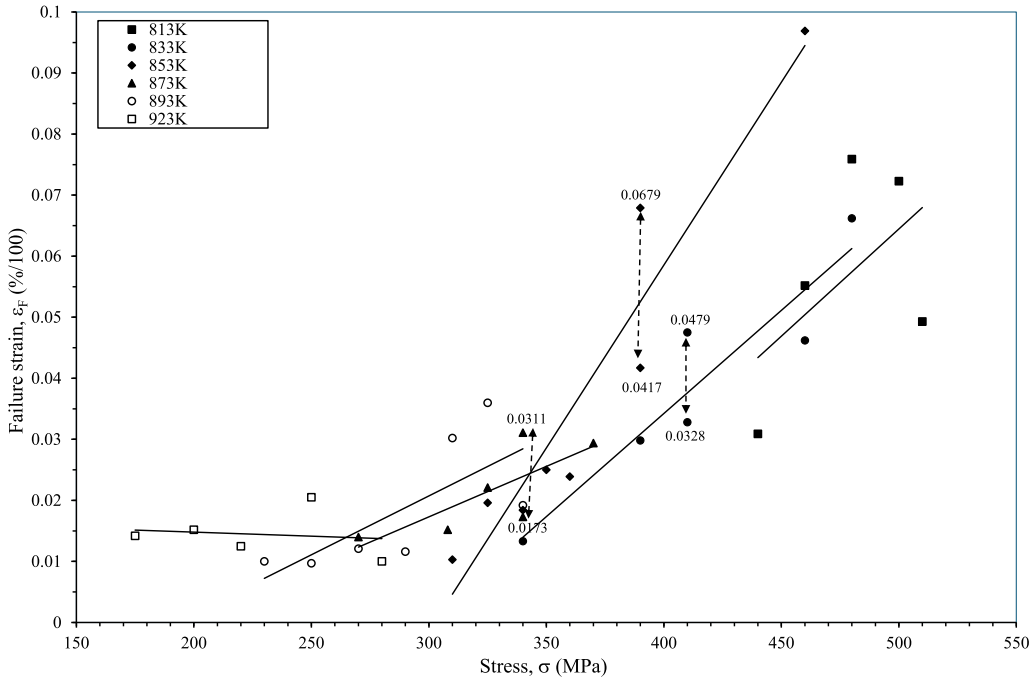

Fig. 7—Variation of strain at failure with stress and temperature, together with unweighted iso-thermal best fit lines.

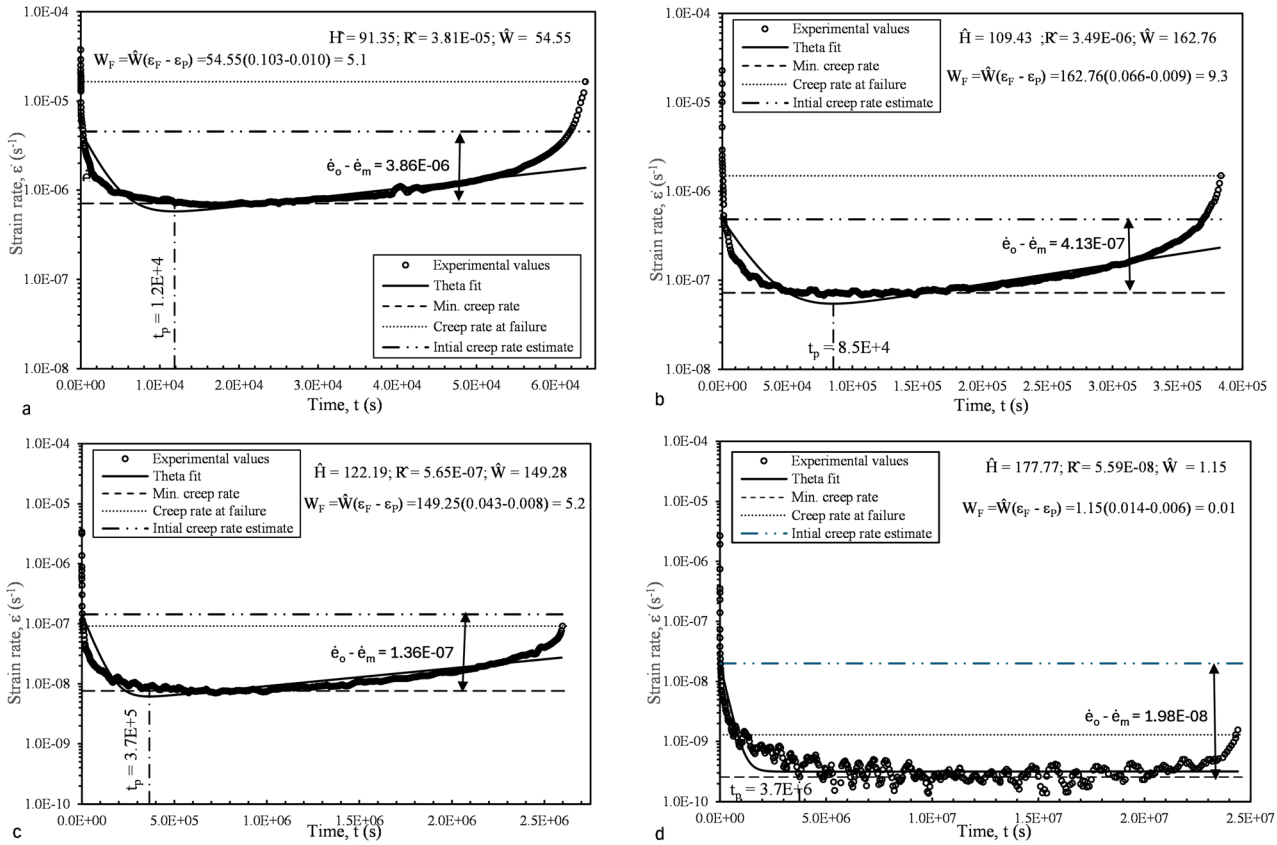

Fig. 8—Variation in strain rate with time at 833 K and at (*a*) 480 MPa, (*b*) 460 MPa, (*c*) 410 MPa, and (*d*) 340 MPa.

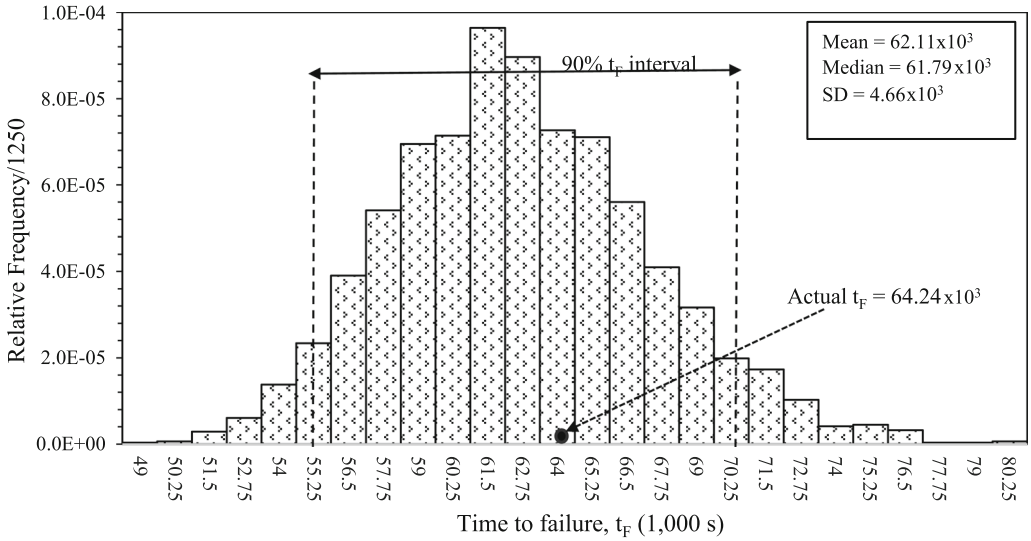

Fig. 9—Frequency histogram of 2500 times to failure obtained at 833 K and 480 MPa.

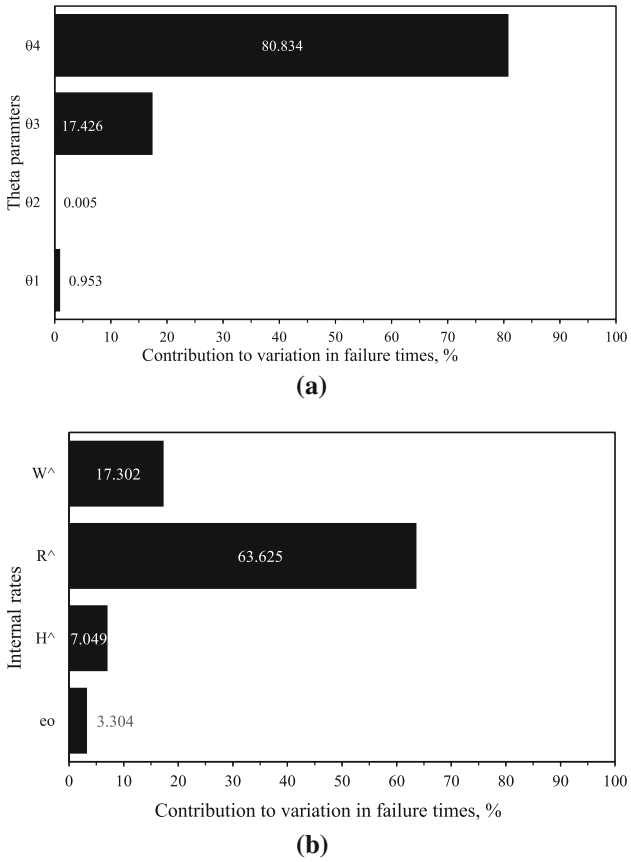

Fig. 10—(*a*) Contribution of each θ_1 to variation in times to failure at 833 K and 480 MPa obtained using method 1. (*b*) Contribution of hardening, softening and damage during creep to variation in times to failure at 833 K and 480 MPa obtained using method 1.

the best that can be said is that $\hat{W}$ and $\hat{R}$ jointly contribute to 83.9 + 7.4 = 91.3 pct of the variation in failure times—they are the main determinants of failure times at this test condition.

The largest value for $\hat{R}$ displayed in Figure 8 is recorded at this test condition leading to the largest total primary strain over the four different tests in this figure and to the time spent in primary creep making up a fifth of the time to failure. This allows primary processes to play a big role in determining when failure eventually occurs.

C. *Decomposition of the Time to Failure at 833K and 410 MPa with Fixed Failure Strain*

Figure 12 plots the 2500 generated failure times at 833K and 410 MPa. The mean of these failure times was 2.81×10^6 seconds (780 hours) with a standard deviation of 30,060s (8.35 hours). At this test condition, the failure time distribution is symmetric, and the actual time to failure is a little above the mean of the distribution. Despite the small size of the standard errors for the theta parameters at this test condition, this transmits into quite a large variation in the times to failure around the mean. A comparison of Figure 13(a) with Figure 10(a) shows that a big change occurs regarding the importance of θ_3 and θ_4 in the determination of time to failure. Essentially the relative importance of these parameters flips as the stress is reduced from 480 MPa to 410 MPa with θ_3 now being the major contributor to variation in time to failure. This test condition has a strong correlation between the softening and damage rates (− 0.65) and between softening and hardening rates (0.73) and this makes it difficult to decompose failure times with respect to these rates.

This complication is seen in Figure 13(b) which shows the contribution of each rate parameter to the failure times as determined by method 1. At first sight, it now appears that the damage rate has the biggest effect on failure times, followed by the softening rate parameter. But the above-mentioned correlation results in the percentage contributions seen in Figure 13(b) summing to more than 100 pct. So, whilst it appears that at this lower stress, damage appears the more important

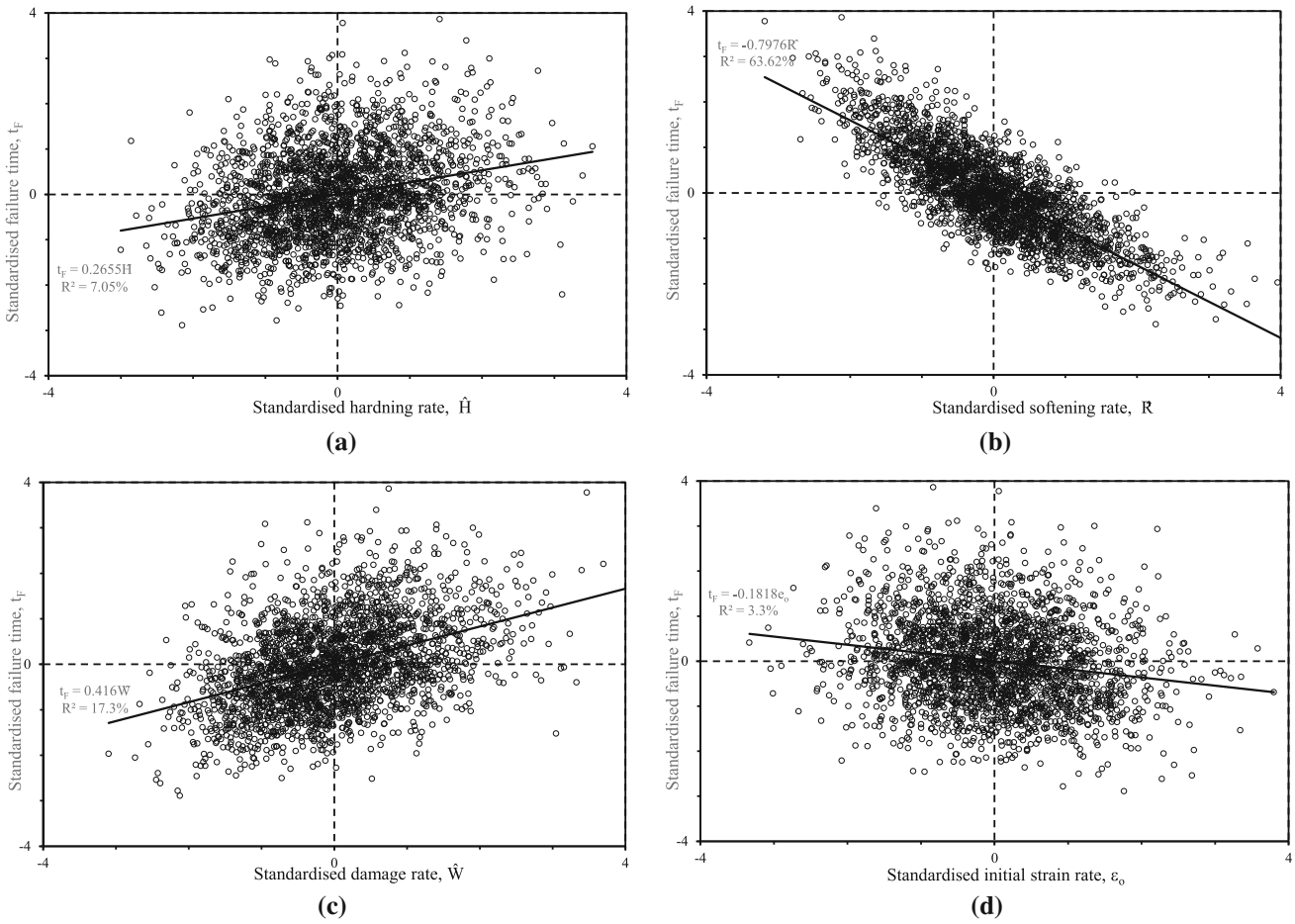

Fig. 11—Variation of standardised failure times, together with best fit lines, with a. the standardised hardening rate, b. the standardised softening rate, c. the standardised damage rate, and d. the initial creep rate at 833K and 480 MPa.

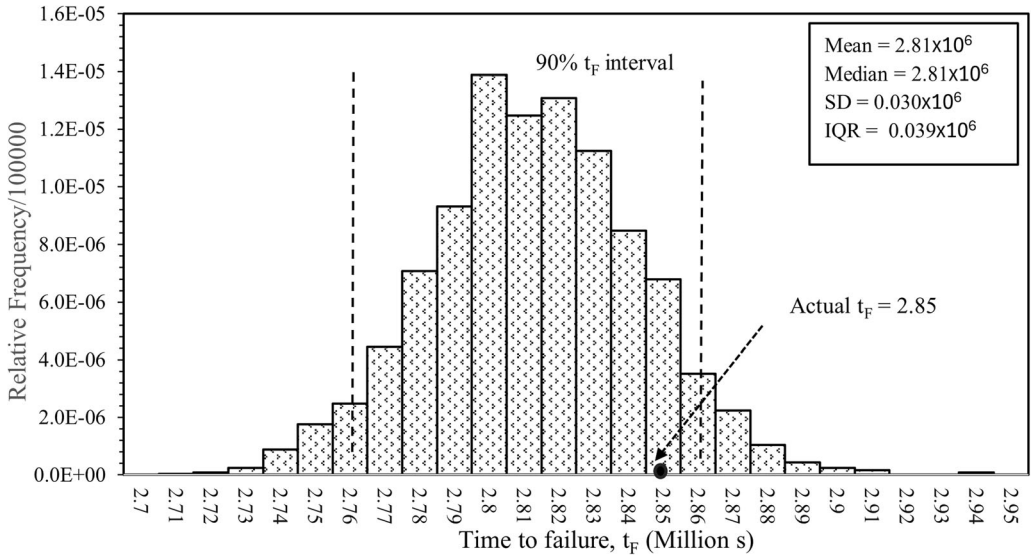

Fig. 12—Frequency histogram of 2500 times to failure at 833 K and 410 MPa.

variable, the percentages should not be interpreted literally. When method 2 is used, the addition of variable $z_{\hat{R},i}$ to Eq. [47] leads to $R^{*2}_{\hat{R}} = 78.4$pct and then when variable $z_{\hat{W},i}$ is finally added, to $R^{*2}_{\hat{W}} = 0.03$ pct. But when $z_{\hat{W},i}$ is added first the following values are

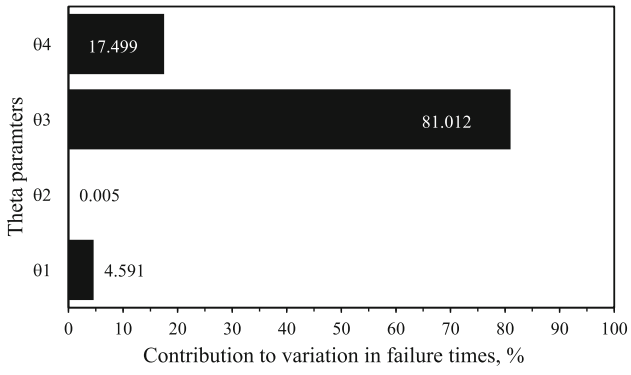

(a)

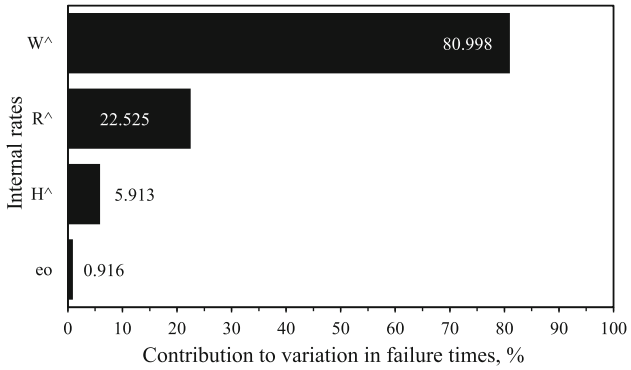

(b)

Fig. 13—(*a*) Contribution of each θ_l to variation in times to failure at 833 K and 410 MPa using method 1. (*b*) Contribution of hardening, softening, and damage during creep to variation in times to failure at 833 K and 410 MPa using method 1.

obtained: $R^{*2}_{\hat{R}} = 0.001$pct with $R^{*2}_{\hat{W}} = 78.39$ pct. Thus, the correct conclusion is that around 78 pct of the variation in times to failure are jointly explained by the damage and softening rate parameters—with damage probably making up the main part of this percentage.

The second part of this last sentence is based on the large contribution from θ_3 shown in Figure 13(a), because the damage rate is inversely proportional to θ_3. It is also based on the best fit lines shown in Figure 14. Whilst the regression of failure times on each variable separately can result in an omission of variable bias, it does produce sensible parameter estimates. For example, when only $z_{\hat{\varepsilon}_{o,i}}$ and $z_{\hat{H},i}$ are included in the regression given by Eq. [51], it was found that $\alpha^*_1 = -0.017$ and $\alpha^*_2 = 0.238$. These are similar in value to the estimates shown in Figures 14(a) and (d) because there is little correlation between the hardening rate and the initial strain rate. But when $z_{\hat{R},i}$ is also included in the regression given by Eq. [51] it was found that $\alpha^*_1 = -0.01$ (little changed), but $\alpha^*_2 = 1.24$ (with $\alpha^*_3 = -1.37$)—which is a very big change due to the hardening and softening rates being highly correlated. This correlation leads to it being impossible to disentangle these two effects when all three internal variables enter Eq. [51]. Therefore, the best fit lines shown in Figure 14, based on individual variables entering the regression, are likely to produce more sensible estimates of all the α values.

The best fit line in Figure 14(a) reveals that a 1 standard deviation increase in the hardening rate (equivalent to a change of 2.94 units) leads to an increase in failure times equal to 24.3 pct of the standard deviation in failure times—equivalent to 7290 seconds (or 2 hours). In comparison to this, Figure 13(b) reveals that a 1 standard deviation increase in the softening rate (equivalent to a change of 1.8×10^{-8} units) leads to a decrease in failure times equal to 47.5 pct of the standard deviation in failure times—or 14,250 million seconds (4 hours). This a much larger effect compared to the effect of changes in the hardening. The effect of changes in the damage rate is even bigger. The best fit line in Figure 13(c) reveals that a 1 standard deviation increase in the damage rate (equivalent to a change of 3.2 units) leads to an increase in failure times equal to 90 pct of the standard deviation in failure times—equivalent to 27,000 million seconds (or 7.5 hours). Figure 14(d) shows that changes in the initial strain rate have the smallest impact of failure times. These estimates reinforce the conclusion that it is the damage rate that is the major contributor failure times at this lower stress. But due to the omission of variables problem, these estimates should be treated as approximate.

D. *Decomposition of the Time to Failure at 833K and 410 MPa with Stochastic Failure Strain*

At this test condition two specimens were put on test resulting in two recorded failure times—2.858×10^6 and 2.6179×10^6 seconds. Notice that this later failure time is outside the range of the failure time distribution shown in Figure 12, suggesting that the strain at failure may be a major contributor to the time to failure. The two corresponding failure strains of 4.75 and 3.28 pct enable this possibility to be studied further. This was done by carrying out the same analysis as in the previous section, but in addition drawing 2500 values of strain at failure from a triangular distribution with limits given by these two strain values. This can be seen as an approximation to the normal distribution (which is not used here as there were only two values present for determining the standard deviation in failure strain). The results are summarised in Figure15, where the two recoded failure times are now contained within the frequency histogram. Compared to Figure 12, the distribution is much wider—as reflected by the higher standard deviation of 117,180 seconds (compared to 30,060 seconds when ε_F is treated as fixed). Interestingly, ε_F explained 94 pct of the variation in times to failure.

E. *Decomposition of the Time to Failure at 833K and 340 MPa*

Figure 16 plots the 2500 generated failure times at 833K and 340 MPa. The mean of these failure times was 24.58×10^6 seconds (6828 hours) with a standard deviation of 387,380 seconds (108 hours). At this test condition, the failure time distribution is skewed to the

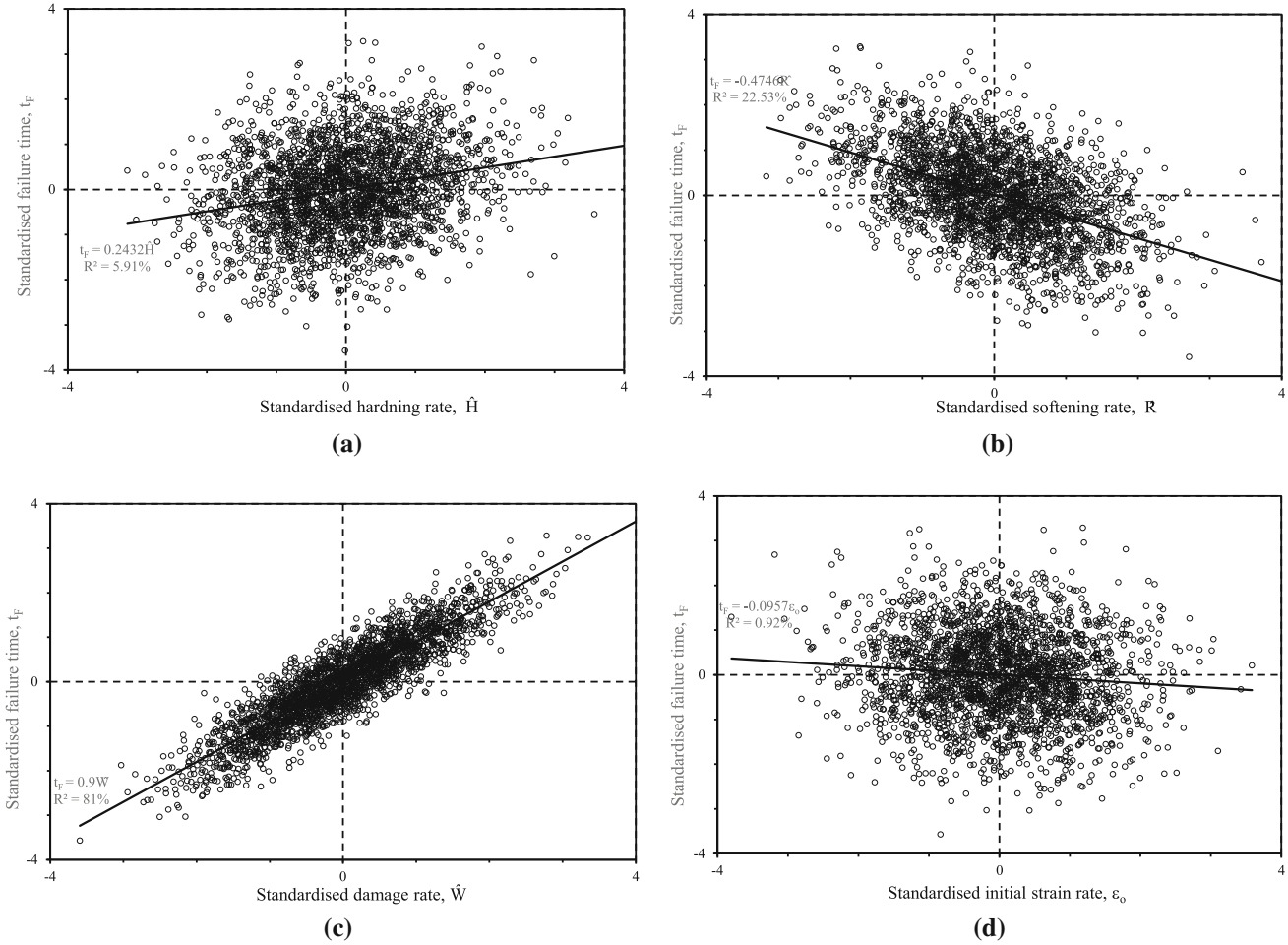

Fig. 14—Variation of standardised failure times, together with best fit lines, with (*a*) the standardised hardening rate, (*b*) the standardised softening rate, (*c*) the standardised damage rate, and (*d*) the initial creep rate at 833K and 410 MPa.

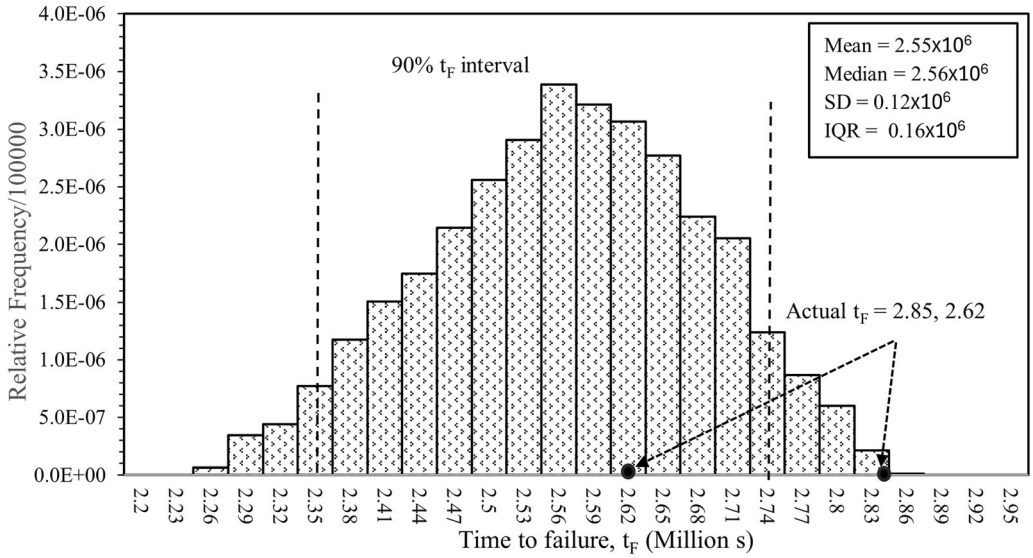

Fig. 15—Frequency histogram of 2500 times to failure at 833 K and 410 MPa when strain at failure follows a triangular distribution.

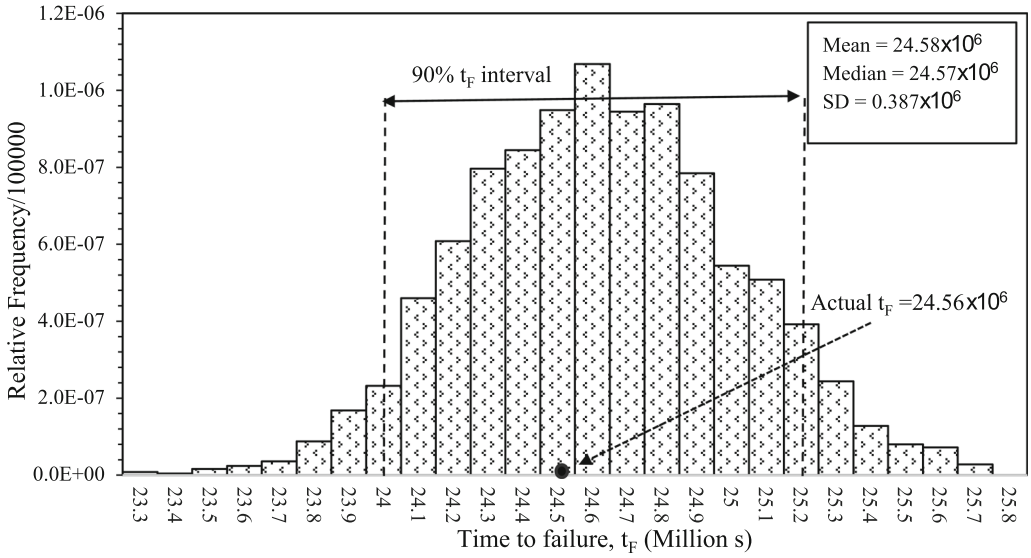

Fig. 16—Frequency histogram of 2500 times to failure at 833K and 340 MPa.

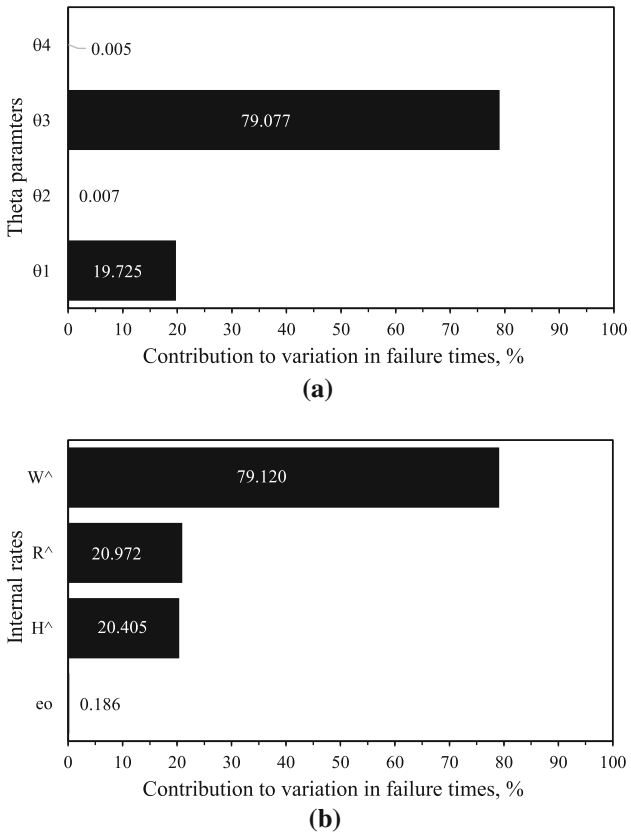

Fig. 17—(*a*) Contribution of each θ_1 to variation in times to failure at 833K and 340 MPa using method 1. (*b*) Contribution of hardening, softening, and damage during creep to variation in times to failure at 833K and 340 MPa using method 1.

left, and the actual time to failure is approximately equal to the mean of the distribution. Despite the small size of the standard errors for the theta parameters at this test condition, this transmits into quite a large variation in the times to failure around the mean. A comparison of Figure 17(a) with Figures 10(a) and 13(a) reveals that with decreasing stress the role played by θ_4 in determining failure times diminishes, whilst the roles of θ_3 and θ_1 increase. The increase in the contribution from θ_1 suggests an increasing role for primary creep in determining time to failure with diminishing stress. Like the previous test condition, this test condition also has a strong correlation between the softening and damage rates (− 0.58) and between softening and hardening rates (0.81) and this makes it difficult to decompose failure times with respect to these rates.

This complication is seen in Figure 17(b) which shows the contribution of each rate parameter to the failure times as determined by method 1. At first sight, it appears that at this test condition it is now the damage rate that has the biggest effect on failure times followed jointly by the softening and hardening parameters. But the above-mentioned correlation results in the percentage contributions seen in Figure 17(b) summing to more than 100 pct. So, whilst it appears that at this lower stress, damage appears the more important variable, the percentages should not be interpreted literally. When method 2 is used, the addition of variable $z_{\hat{H},i}$ to Eq. [47] leads to $R^{*2}_{\hat{H}} = 21.4\,\text{pct}$, then the addition of variable $z_{\hat{R},i}$ to Eq. [47] leads to $R^{*2}_{\hat{R}} = 0.001\,\text{pct}$ and then when variable $z_{\hat{W},i}$ is finally added to $R^{*2}_{\hat{W}} = 0.03$ pct. But when $z_{\hat{W},i}$ is added before $z_{\hat{R},i}$, the following values are obtained: $R^{*2}_{\hat{H}} = 21.4\,\text{pct}$, $R^{*2}_{\hat{R}} = 78.39\,\text{pct}$ with $R^{*2}_{\hat{W}} = 78.39$ pct. Thus, the correct conclusion is that around 78 pct of the variation in times to failure is jointly explained by the damage and softening parameters, with damage probably making up the main part of this percentage.

Again, the second part of this conclusion is based on the large contribution from θ_3 seen in Figure 17(a) and from the best fit lines shown in Figure 18. The regression of failure times on each variable separately does produce

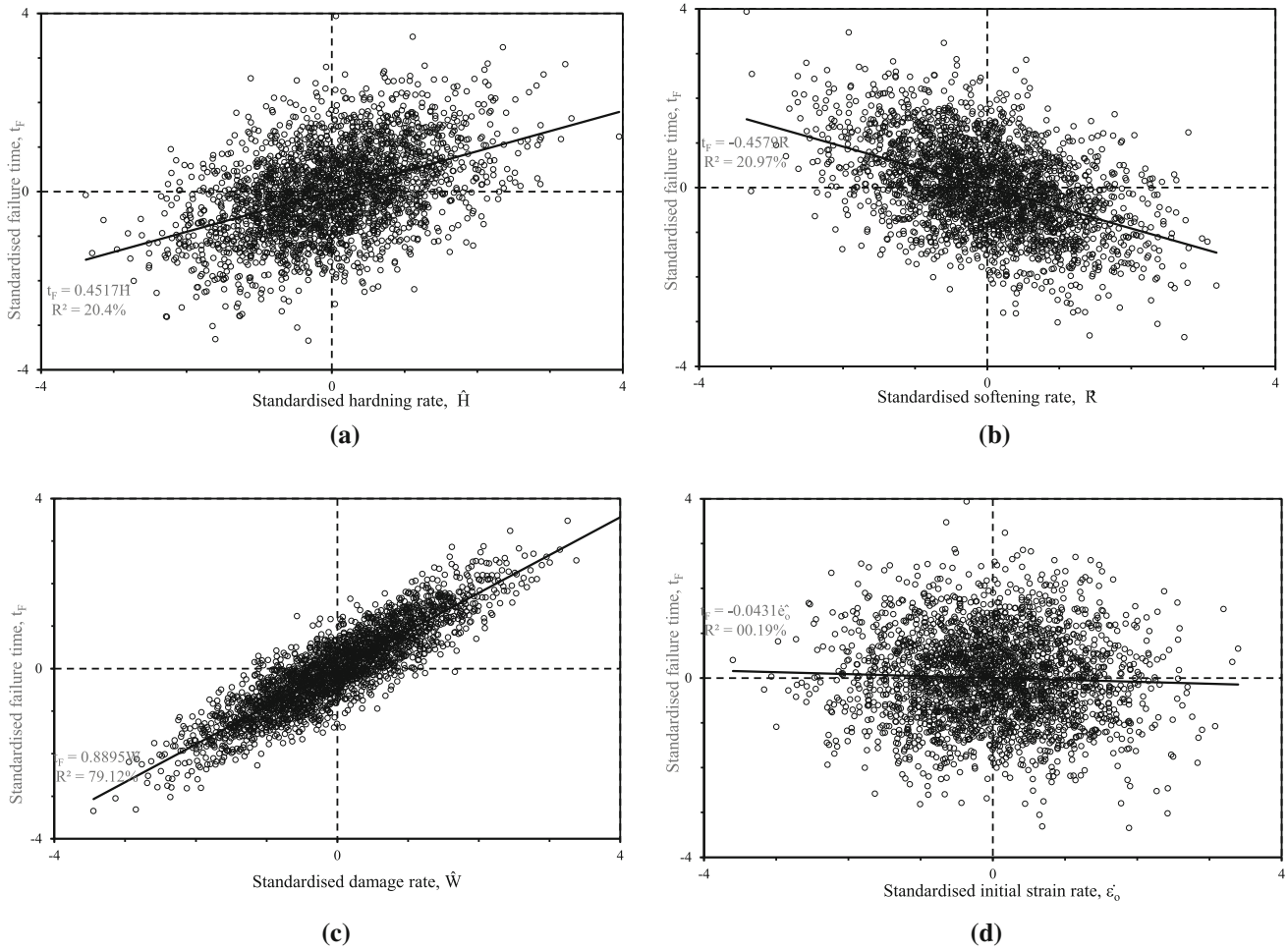

Fig. 18—Variation of standardised failure times, together with best fit lines, with (*a*) the standardised hardening rate, (*b*) the standardised softening rate, (*c*) the standardised damage rate, and (*d*) the initial creep rate at 833K and 340 MPa.

sensible parameter estimates. For example, when only $z_{\dot{\varepsilon}_{o,i}}$ and $z_{\hat{H},i}$ are included in the regression given by Eq. [51], it was found that $\beta^*_1 = -0.11$ and $\beta^*_2 = 0.467$. These are similar in value to the estimates shown in Figures 18(a) and (d), because there is little correlation between the hardening rate and the initial strain rate. But when $z_{\hat{R},i}$ is also included in the regression given by Eq. [51], it was found that $\beta^*_1 = -0.10$ (little changed), but $\beta^*_2 = 1.10$ (with $\beta^*_3 = -1.09$)—which is a very big change that is due to hardening and softening rates being highly correlated. This correlation leads to it being impossible to disentangle these two effects when all three variables enter Eq. [51]. Therefore, the best fit lines shown in Figure 18 based on individual variables entering the regression are likely to produce more sensible estimates of all the β values.

Based on this, the best fit line in Figure 18(a) reveals that a 1 standard deviation increase in the hardening rate (equivalent to a change of 1.82 units) leads to an increase in failure times equal to 45.2 pct of the standard deviation in failure times—equivalent to 0.175×10^6 seconds (or 49 hours). In comparison to this, Figure 18(b) reveals that a 1 standard deviation increase in the softening rate (equivalent to a change of 9.74×10^{-10} units) leads to a decrease in failure times equal to 45.8 pct of the standard deviation in failure times—or 0.177×10^6 seconds (50 hours). This is similar to the effect of changes in the hardening rate. The effect of changes in the damage rate is however much bigger. The best fit line in Figure 18(c) reveals that a 1 standard deviation increase in the damage rate (equivalent to a change of 0.02 units) leads to an increase in failure times equal to 88.9 pct of the standard deviation in failure times—equivalent to 0.344×10^6 seconds (or 96 hours). Figure 18(d) shows that changes in the initial strain rate have the smallest impact of failure times. These estimates reinforce the conclusion that it is the damage rate that is the major contributor failure times at this lower stress. But due to the omission of variables problem, these estimates should be treated as approximate.

V. CONCLUSION

This paper has derived an equation for the relationships between time to failure and minimum creep rates using a 4-θ description of a creep curve obtained under

constant tests conditions. The four θ parameters were then related to rates of hardening, softening, and damage. It was found that the exponent on $\dot{\varepsilon}_m$ was predicted by the 4-θ methodology to have a value of -1. The 4-θ methodology also predicted that the Monkman–Grant proportionality constant (M in Eq. [1]) depended negatively on the rate of damage accumulation, the initial strain rate (for virgin material) and the rate of hardening, but positively on the strain at failure and $\dot{\varepsilon}_m$ itself. All these variables were also shown to depend on test conditions, so that M is not really a constant. Consequently, measuring values for $\dot{\varepsilon}_m$ will offer limited capabilities in predicting long-term creep rupture, unless a clear and well-defined relationship between test conditions and $\hat{H}$, $\hat{W}$, $\hat{R}$, ε_F, and $\dot{\varepsilon}_o$ can be identified. Allowing for the variability observed in strain at failure increased the standard deviation in failure times from 30,060 to 117,181 seconds. This also cast doubt on the ability of the Monkman–Grant relation to be able to produce reliable long-term creep life predictions.

The paper then goes on to use this relation to quantify the contribution of creep hardening, softening, and damage to variations in the time to failure using simulation techniques. It was found that at 833K and a high stress, θ_4 was the major determinant of failure times. But as the stress level fell, the parameters θ_3 and θ_1 became more important. The growing importance of θ_3 with decreasing stress implies a bigger role for damage accumulation with decreasing stress (as $\hat{W} = 1/\theta_3$). This was confirmed in this paper where at the highest stress, the rate of softening was the biggest contributor to variations in failure time. At lower stresses the role of the damage rate and the hardening rate become jointly more important. Areas for future work include research into finding out whether these conclusions hold for some other materials, and when studying very ductile materials, whether a 6-θ methodology would reveal further insights.

FUNDING

No financial or non-financial assistance was provided by a third party for the reported work. There are no financial interest or relationship—*within the last 3 years*—related to the subject matter but not directly to this manuscript. There are no patents or copyrights that are relevant to the work in the manuscript. There is nothing else of merit to declare.

COMPETING INTERESTS

On behalf of all authors, the corresponding author states that there is no conflict of interest

APPENDIX

At constant stress and temperature, $\hat{H}, \hat{R},$ and $\hat{W}$ are also constant, and if H = R = W = 0, when t = 0, then the differential of Eq. (16) with respect to time is

$$\ddot{\varepsilon} = \dot{\varepsilon}_o\left[\dot{H} + \dot{R} + \dot{W}\right] = \dot{\varepsilon}_o\left[\hat{R} + \left(\hat{W} - \hat{H}\right)\dot{\varepsilon}\right]. \quad [54]$$

Carrying out the following integration

$$\int_{\dot{\varepsilon}_o}^{\dot{\varepsilon}} \frac{1}{\hat{R} + \left(\hat{W} - \hat{H}\right)\dot{\varepsilon}} d\dot{\varepsilon} = \dot{\varepsilon}_o \int_0^t dt \quad [55]$$

gives

$$\ln\left[\hat{R} + \left(\hat{W} - \hat{H}\right)\dot{\varepsilon}\right] + C = \left(\hat{W} - \hat{H}\right)\dot{\varepsilon}_o t, \quad [56]$$

where C is the constant of integration. When t = 0, $\dot{\varepsilon} = \dot{\varepsilon}_o$ and so C = -ln($\left(\hat{R} + \left(\hat{W} - \hat{H}\right)\dot{\varepsilon}_o\right)$. Substituting this value for C into Eq. [55] gives

$$\ln\left[\frac{\hat{R} + \left(\hat{W} - \hat{H}\right)\dot{\varepsilon}}{\hat{R} + \left(\hat{W} - \hat{H}\right)\dot{\varepsilon}_o}\right] = \left(\hat{W} - \hat{H}\right)\dot{\varepsilon}_o t \quad [57]$$

which upon rearrangement and simplification yields

$$\dot{\varepsilon} = \left[\dot{\varepsilon}_o + \frac{\hat{R}}{\left(\hat{W} - \hat{H}\right)}\right] e^{\left(\hat{W} - \hat{H}\right)\dot{\varepsilon}_o t} - \frac{\hat{R}}{\left(\hat{W} - \hat{H}\right)}. \quad [58]$$

The creep curves in Figure 1 are characterised by a short period of primary creep, (t_M is small) during which there is a rapidly decline rate of creep. They are also characterised by small rates of acceleration in the creep rate at the end of secondary creep. For Eq. [58] to have these characteristics $\left(\hat{W} - \hat{H}\right) < 0$. Then, at the start of a creep test (t = 0), the rate of strain is given by $\dot{\varepsilon}_o$ (as $e^o = 1$) and subsequently, $\dot{\varepsilon}$ will reduce in value until a value of $\frac{\hat{R}}{\left(\hat{W} - \hat{H}\right)}$ is reached. This is the minimum or secondary creep rate, the value of which depends on the rates for hardening, recovery, and damage. But for this to happen rapidly, $\hat{W}$ must also be very small relative to $\hat{H}$. This is the reasoning behind the assumptions made by Evans, that damage accumulation in minimal during primary creep, *i.e.* $-\frac{\hat{R}}{\left(\hat{W} - \hat{H}\right)}$ approximately equals $\frac{\hat{R}}{\hat{H}}$ and so can be replaced by $\frac{\hat{R}}{\left(\hat{H}\right)}$ in Eq. [58]. Then, primary and secondary creep can be modelled as

$$\dot{\varepsilon} = \left[\dot{\varepsilon}_o - \frac{\hat{R}}{\hat{H}}\right] e^{-\hat{H}\dot{\varepsilon}_o t} + \frac{\hat{R}}{\hat{H}}. \quad [59]$$

This does not mean that damage does not occur during the time that primary creep occurs, but only that this is dominated by the rate of hardening so that the contribution of damage to decaying creep rates in primary creep is small.

Then, damage is assumed to influence this secondary creep rate during tertiary creep

$$\dot{\varepsilon}_T = \frac{\hat{R}}{\hat{H}}[1 + W], \qquad [60]$$

where $\dot{\varepsilon}_T$ is the tertiary strain rate. This can be rewritten in terms of time t by first noting that
$\ddot{\varepsilon}_T = \frac{\hat{R}}{\hat{H}}[\dot{W}] = \frac{\hat{R}}{\hat{H}}\hat{W}\dot{\varepsilon}_T$
so that

$$\int \frac{1}{(\hat{W}\dot{\varepsilon}_T)} d\dot{\varepsilon}_T = \frac{\hat{R}}{\hat{H}} \int dt.$$

Thus
$\frac{1}{\hat{W}} \ln[\dot{\varepsilon}_T] = \frac{\hat{R}}{\hat{H}} t + C$
with $C \cong \frac{1}{\hat{W}} \ln\left[\frac{\hat{R}}{\hat{H}}\right]$ (approximate because the creep rate equals the secondary rate when $t = t_M$, but assuming t_M is small (as in Figure 1) it follows that the creep rate equals the secondary rate when t is approximately zero). Upon further simplification,

$$\dot{\varepsilon}_T = \frac{\hat{R}}{\hat{H}} e^{\frac{\hat{W}\hat{R}}{(\hat{H})}t}.$$

Substituting this into Eqs. [19, 59] gives

$$\dot{\varepsilon} = \left[\dot{\varepsilon}_o - \frac{\hat{R}}{\hat{H}}\right] e^{-\hat{H}\dot{\varepsilon}_o t} + \frac{\hat{R}}{\hat{H}} e^{\frac{\hat{W}\hat{R}}{\hat{H}}t}. \qquad [61]$$

The equivalent expression in terms of the θ values is

$$\dot{\varepsilon} = \theta_1\theta_2 e^{\theta_2 t} + \theta_3\theta_4 e^{\theta_4 t},$$

where $\theta_2 < 0$. When $t = 0$, $\dot{\varepsilon} = \dot{\varepsilon}_0$ and so

$$\dot{\varepsilon}_0 = \theta_1\theta_2 + \theta_3\theta_4.$$

Thus $\theta_3\theta_4 = \frac{\hat{R}}{\hat{H}}$, $\theta_4 = \frac{\hat{W}\hat{R}}{\hat{H}}$ and so $\theta_3 = \frac{\theta_3\theta_4}{\theta_4} = \frac{1}{\hat{W}}$
Similarly,
$\theta_2 = \hat{H}\dot{\varepsilon}_o$ and so $\hat{H} = \frac{\theta_2}{\theta_1\theta_2 + \theta_3\theta_4}$.
Finally, $\hat{R} = \frac{\theta_2\theta_3\theta_4}{\theta_1\theta_2 + \theta_3\theta_4}$
θ_3 determines the rate of damage accumulation $\hat{W}$. But θ_3 also determines in part the values for $\hat{R}$ and $\dot{\varepsilon}_o$ and thus also $\hat{H}$. So, it follows that the rate of damage accumulation also controls primary creep. Thus, the assumptions made in the above derivations only restrict damage generation to those strains arising from the secondary process, which is present throughout the whole of primary. Damage is therefore influenced by what happens during primary creep.

The Integral of Eq. [61] gives the equation for a uniaxial creep curve, and this can be carried in two parts:

Part 1.

$$\int \left[\dot{\varepsilon}_o - \frac{\hat{R}}{\hat{H}}\right] e^{-\hat{H}\dot{\varepsilon}_o t} dt = \left[\dot{\varepsilon}_o - \frac{\hat{R}}{\hat{H}}\right] \int e^{-\hat{H}\dot{\varepsilon}_o t} dt. \qquad [62]$$

But

$$\int e^{-\hat{H}\dot{\varepsilon}_o t} dt = \frac{1}{-\hat{H}\dot{\varepsilon}_o} e^{-\hat{H}\dot{\varepsilon}_o t} \qquad [63]$$

and so

$$\int \left[\dot{\varepsilon}_o - \frac{\hat{R}}{\hat{H}}\right] e^{-\hat{H}\dot{\varepsilon}_o t} dt = -\frac{\dot{\varepsilon}_o - \frac{\hat{R}}{\hat{H}}}{\hat{H}\dot{\varepsilon}_o} e^{-\hat{H}\dot{\varepsilon}_o t}. \qquad [64]$$

Part 2.

$$\int \frac{\hat{R}}{\hat{H}} e^{\frac{\hat{W}\hat{R}}{\hat{H}}t} dt = \frac{\hat{R}}{\hat{H}} \int e^{\frac{\hat{W}\hat{R}}{\hat{H}}t} dt = \frac{\hat{R}}{\hat{H}} \frac{\hat{H}}{\hat{W}\hat{R}} e^{\frac{\hat{W}\hat{R}}{\hat{H}}t} = \frac{1}{\hat{W}} e^{\frac{\hat{W}\hat{R}}{\hat{H}}t}. \qquad [65]$$

Combining Eqs. [64] and [65] gives

$$\int \dot{\varepsilon} dt = \varepsilon = C - \frac{\dot{\varepsilon}_o - \frac{\hat{R}}{\hat{H}}}{\hat{H}\dot{\varepsilon}_o} e^{-\hat{H}\dot{\varepsilon}_o t} + \frac{1}{\hat{W}} e^{\frac{\hat{W}\hat{R}}{\hat{H}}t}, \qquad [66]$$

where C is the integration constant. When $t = 0$, $\varepsilon = 0$, and so

$$C = \frac{\dot{\varepsilon}_o - \frac{\hat{R}}{\hat{H}}}{\hat{H}\dot{\varepsilon}_o} - \frac{1}{\hat{W}}. \qquad [67]$$

Substituting Eqs. [67] into [66] gives

$$\varepsilon = -\frac{1}{\hat{H}\dot{\varepsilon}_o}\left[\dot{\varepsilon}_o - \frac{\hat{R}}{\hat{H}}\right]\left(1 - e^{-\hat{H}\dot{\varepsilon}_o t}\right) + \frac{1}{\hat{W}}\left(e^{\frac{\hat{W}\hat{R}}{\hat{H}}t} - 1\right), \qquad [68]$$

which is Eq. [23] in the main text.

OPEN ACCESS

REFERENCES

1. M. Yang, Q. Wang, X.L. Song, J. Jia, and Z.D. Xiang: *Int. J. Mater. Res.*, 2016, vol. 107(2), pp. 133–38.
2. B. Wilshire and A.J. Battenbough: *Mater. Sci. Eng. A*, 2007, vol. 443, pp. 156–66.

3. B. Wilshire and P.J. Scharning: *Mater. Sci. Technol.*, 2008, vol. 24(1), pp. 1–9.
4. B. Wilshire and M. Whittaker: *Mater. Sci. Technol.*, 2001, vol. 27(3), pp. 642–47.
5. B. Wilshire and P.J. Scharning: *Int. Mater. Rev.*, 2008, vol. 53(2), pp. 91–104.
6. M.T. Whittaker, M. Evans, and B. Wilshire: *Mater. Sci. Eng., A*, 2012, vol. 552, pp. 145–50.
7. F.C. Monkman and N.J. Grant: *Proc. Am. Soc. Test. Mater.*, 1956, vol. 56, pp. 593–620.
8. M. Evans: *Mater. High Temp.*, 2022, vol. 39(2), pp. 133–48.
9. F. Abe: *Metall. Mater. Trans.*, 2003, vol. 34A, pp. 913–25.
10. K. Maruyama, N. Sekido, and K. Yoshimi: *Mater. Sci. Eng., A*, 2019, vol. 749, pp. 223–34.
11. F. Dobes and K. Milicka: *Metal. Sci.*, 1976, vol. 10, pp. 382–84.
12. V. Sklenicka, K. Kucharova, P. Kral, M. Kvapilova, and J. Dvorak: *Kov. Mater.*, 2017, vol. 55, pp. 69–80.
13. R. W. Evans and B. Wilshire. *Creep of Metals and Alloys*, Institute of Metals, London, Appendix, 1985.
14. R.W. Evans: *R. Soc. Proc. Math. Phys. Eng. Sci.*, 1996, vol. 2000(456), pp. 835–68.
15. F. Kafexhiu, F. Vodopivec, and B. Podgornik: *Metalurgija*, 2017, vol. 56(3–4), pp. 353–56.
16. R.W. Evans: *Mater. Sci. Technol.*, 1989, vol. 5(7), pp. 699–707.
17. W.K. Newey and K.D. West: *Econometrica*, 1987, vol. 55(3), pp. 703–08.
18. M. Evans: *J. Strain Anal. Eng. Des.*, 2002, vol. 37(2), pp. 169–83.
19. M. Matsumoto and T. Nishimura: *ACM Trans. Model. Comput. Simul.*, 1998, vol. 8(1), pp. 3–30.
20. H. Han, J. Shen, and J. Xie: *Sci. Rep.*, 2018, vol. 8, p. 15411.
21. J. Pešička, A. Ghajani, Ch. Somsen, A. Hartmaier, and G. Eggeler: *Scr. Mater.*, 2010, vol. 62(6), pp. 353–56.
22. N. Dudova: *Metals*, 2022, vol. 12(7), p. 1119.
23. J. Parker: Component Relevant Creep Damage in Tempered Martensitic 9 to 12 %Cr Steels. In *Advances in Materials Technology for Fossil Power Plants:* Proceedings from the Eighth International Conference, Algarve- Portugal, 2016.